Oligoclonal nanobody-based recombinant antivenom for cobra, mamba, and rinkhals bites

Shirin Ahmadi[1]*, Nick J. Burlet[1]*, Melisa Benard-Valle[1], Alid Guadarrama-Martínez[2], Samuel Kerwin[3], Iara A. Cardoso[4,5], Amy E. Marriott[6], Rebecca J. Edge[6], Edouard Crittenden[4], Edgar Neri-Castro[2], Monica L. Fernandez-Quintero[7], Giang T. T. Nguyen[1], Carol O'Brien[1], Yessica Wouters[1], Konstantinos Kalogeropoulos[1], Suthimon Thumtecho[1], Tasja Wainani Ebersole[1], Camilla Holst Dahl[1], Emily U. Glegg-Sørensen[1], Tom Jansen[1], Kim Boddum[8], Evangelia Manousaki[1], Esperanza Rivera-de-Torre[1], Andrew B. Ward[7], J. Preben Morth[1], Alejandro Alagón[2], Stephen P. Mackessy[3], Stuart Ainsworth[6], Stefanie K. Menzies[9], Nicholas R. Casewell[4], Timothy P. Jenkins[1#], Anne Ljungars[1#], Andreas H. Laustsen[1#]

[1]Department of Biotechnology and Biomedicine, Technical University of Denmark, DK-2800 Kongens Lyngby, Denmark

[2]Departamento de Medicina Molecular y Bioprocesos, Instituto de Biotecnología, Universidad Nacional Autónoma de México, Avenida Universidad 2001, Cuernavaca, Mor., 62210, México

[3]Department of Biological Sciences, University of Northern Colorado, 501 20th St., CB 92, Greeley, CO 80639-0017, USA

[4]Centre for Snakebite Research and Interventions, Department of Tropical Disease Biology, Liverpool School of Tropical Medicine, Pembroke Place, Liverpool, L3 5QA, United Kingdom

[5]School of Biochemistry, University of Bristol, Biomedical Sciences Building, University Walk, Bristol, BS8 1TD, United Kingdom

[6]Department of Infection Biology and Microbiomes, Institute of Infection, Veterinary and Ecological Sciences, University of Liverpool, Liverpool, L3 5RF, United Kingdom

[7]Department of Integrative Structural and Computational Biology, The Scripps Research Institute, La Jolla, CA, USA

[8]Sophion Bioscience, DK-2750 Ballerup, Denmark

[9]Biomedical & Life Sciences, Faculty of Health and Medicine, Lancaster University, Lancaster, LA1 4YG, United Kingdom

[*]Equal contributions

[#]Corresponding authors: Timothy P. Jenkins tpaje@dtu.dk, Anne Ljungars aellj@dtu.dk, and Andreas H. Laustsen ahola@bio.dtu.dk

Abstract

Each year, snakebite envenoming claims thousands of lives and causes severe injury to countless victims across sub-Saharan Africa, many of whom depend on animal plasma-derived antivenoms as their sole treatment option. Unfortunately, traditional antivenoms are expensive, can cause adverse immunological reactions, offer limited efficacy against local tissue damage, and often fail to be effective against all medically relevant snake species. There is thus an urgent unmet medical need for innovation in snakebite envenoming therapy. However, developing broad-spectrum treatments is highly challenging due to the vast diversity of venomous snakes and the complex and variable composition of their venoms. In this study, we addressed this challenge by immunizing camelids with the venoms of 18 different snakes including mambas, cobras, and a rinkhals, constructing phage display libraries, and identifying high-affinity broadly-neutralizing nanobodies. 8 of these nanobodies were combined into a defined oligoclonal mixture, resulting in an experimental polyvalent recombinant antivenom capable of neutralizing 7 toxin (sub)families. This antivenom effectively prevented venom-induced lethality *in vivo* across 17 African elapid snake species and effectively reduced venom-induced dermonecrosis of all cytotoxic venoms tested. The recombinant antivenom performed better than a currently used plasma-derived antivenom and therefore shows considerable promise for comprehensive, continent-wide protection against snakebites by all medically relevant African elapids.

Main

Snakebite envenoming is a neglected tropical disease that disproportionately affects populations in rural tropical regions, with sub-Saharan Africa bearing a significant burden. It is estimated that more than 300,000 snakebites occur annually in this region, leading to over 7,000 deaths and 10,000 amputations, although the actual incidence and mortality may be up to 5 times higher (Fig. 1a).[1,2] Currently, the only specific treatment for snakebite envenoming is antivenoms derived from the plasma of hyperimmunized large animals, such as horses. While life-saving, these antivenoms suffer from batch-to-batch variation, high production costs, sometimes restricted efficacy across species (i.e., limited polyvalency), and the risk of causing immunological adverse reactions.[3-5] In addition, existing antivenoms may contain as little as 10% active ingredient, i.e. antibodies specifically targeting venom toxins.[6] Consequently, large

doses need to be administered, increasing treatment costs. Furthermore, current antivenoms are often ineffective in mitigating local tissue damage caused by envenoming, such as dermonecrosis, which contributes to the high number of amputations and tissue debridement procedures among snakebite victims.[7-9]

To overcome the limitations of current antivenoms, the development of alternative broad-spectrum antivenoms, with a high content of therapeutically active antibodies, and improved efficacy against both lethality and local tissue damage, is critically warranted. To this end, recombinant monoclonal broadly-neutralizing antibodies have shown great promise.[10] Specifically, it has been demonstrated that a single broadly-neutralizing antibody targeting a specific toxin (sub)family can prevent toxicity and/or lethality in mice injected with whole venoms predominantly composed of toxins from that same (sub)family.[11-17] In addition, mixtures of a few recombinant monoclonal antibodies or antigen-binding fragments of camelid heavy-chain-only antibodies, V_HHs (nanobodies), were able to neutralize at least 1 or 2 venoms.[18-21] However, to truly qualify as an alternative to existing therapy, a recombinant antivenom must effectively neutralize venoms from all medically relevant snake species within a region, across different genera. This is particularly challenging to achieve due to the complex compositions of snake venoms, where the venom from a single species can contain up to a hundred toxins from multiple different protein families,[22] which can vary extensively both inter- and intraspecifically.[23] This complexity has created a prevailing view that neutralizing all medically relevant toxins will require an impractically large number of antibodies.

In this work, we demonstrate that neutralization of 17 out of the 18 most medically relevant elapid snakes in sub-Saharan Africa can be achieved with a surprisingly low number of broadly neutralizing toxin-targeting V_HHs. After identifying the medically relevant toxins in the venoms of the 18 elapid snakes (mambas, cobras, rinkhals), we used phage display technology[24,25] to discover V_HHs that were evaluated for their ability to bind and neutralize their target toxins (Fig. 1b). We then designed an experimental recombinant antivenom based on an oligoclonal mixture of the top 8 V_HHs and demonstrated that this antivenom can preclinically prevent venom-induced lethality against all of the 18 most medically relevant elapid snakes in sub-Saharan Africa, except *Dendroaspis angusticeps,* in pre-incubation experiments. We further validated the efficacy of the antivenom using a representative panel of 11 venoms in a more stringent rescue model that better simulates a real-world snakebite scenario. We also demonstrate that the recombinant antivenom can inhibit or reduce morbidity-causing venom-induced dermonecrosis, a previously unexplored therapeutic area for V_HHs.

Collectively, this study demonstrates the feasibility of developing a polyvalent recombinant antivenom with continent-wide species coverage, offering hope for advancing such snakebite envenoming therapeutics to future clinical application.

Discovery of V_HHs against elapid toxins

Africa is inhabited by a plethora of venomous snake species, primarily belonging to the viperid or elapid families; however, many are of no or little medical concern. As outlined by the World Health Organization (WHO), within sub-Saharan Africa there are a total of 18 elapid snakes that can be considered the most medically important (Fig. 1a, Supplementary Table 1).[26,27] They belong to 3 genera: *Dendroaspis* (mambas; 4 species), *Hemachatus* (rinkhals; 1 species), and *Naja* (cobras; 13 species), with the genus *Naja* further being divided into 3 subgenera, i.e. *Uraeus* (cape cobras; 5 species), *Boulengerina* (forest/water cobras; 1 species), and *Afronaja* (African spitting cobras; 7 species). The clinical manifestations of envenoming vary significantly among these 5 (sub)genera. Species belonging to *Dendroaspis, Uraeus,* and *Boulengerina* primarily induce neurotoxic symptoms, while species belonging to *Hemachatus* and *Afronaja* mostly cause severe local tissue damage (Fig. 1c).[28] Neutralizing the wide range of toxic effects that underlie these manifestations is thus no small endeavor, which complicates the development of effective therapies with broad coverage of syndromes and snake species.[29] To discover V_HHs targeting toxins from these venoms, we first generated immune V_HH-displaying phage libraries from 2 camelids injected with a mixture of the above-mentioned 18 elapid venoms (Fig. 1b). Injection doses were increased across bi-weekly intervals over 8 time points, and 3 additional booster injections were administered 52, 54, and 60 weeks after the first immunization.[20] We collected blood samples at different time points during the immunization time course to generate 3 unique V_HH-displaying phage libraries (Supplementary Table 2).

We next identified the most medically relevant toxins present in the 18 elapid venoms based on our previous work.[30] These toxins belong to 3 distinct protein families: three-finger toxins (3FTx), phospholipase A_2s (PLA_2), and Kunitz-type serine protease inhibitors (KUN). The toxins were purified using reversed-phase high-performance liquid chromatography (RP-HPLC) followed by proteomic analysis of the 47 fractions in which the key toxins were expected to be present (Supplementary Fig. 1, Supplementary Table 1). The most abundant 3FTx found in these fractions belonged to 5 different subfamilies, namely the Type I α-neurotoxin (sNTx), Type II α-neurotoxin (lNTx), Type IA/IB cytotoxin (CTx), Orphan group XI (Og XI), and aminergic toxin (AgTx).[31-33] In this study, fractions and purified toxins are

denoted by the name of the main medically relevant toxin (sub)family present in the fraction, followed by a number (e.g. lNTx-1, lNTx-2, etc.) for ease of reference (Supplementary Table 1).

Overall, 16 fractions (3 lNTx, 3 sNTx, 2 KUN, 2 Og XI, 1 AgTx, 1 PLA_2, and 4 CTx) were selected to be used as targets in subsequent phage display selections, based on their abundance in the corresponding venom and their purity (Supplementary Table 3, Supplementary Table 1, Supplementary Fig. 2). Throughout the phage display campaigns, we employed cross-panning strategies[34,35], including e.g. exposure to sNTx fractions from different snake species, and/or decreasing antigen concentrations in consecutive rounds to enrich for V_HHs with broad cross-reactivity and/or high affinity (Supplementary Table 3).

V_HHs demonstrate broad neutralization *in vitro*

Following the phage display campaigns, we subcloned 15 phage pool outputs, expressed over 3,000 monoclonal V_HHs in *E. coli*, and screened them for binding to their cognate target toxins using an expression-normalized capture dissociation-enhanced lanthanide fluorescence immunoassay (DELFIA). Approximately 60% of the V_HHs bound to their target toxins (Fig. 2a), and 25% of the clones with varying signal intensity were tested for cross-reactivity in a secondary DELFIA-based screening. Here, we observed that over 50% of the V_HHs bound multiple toxins from the same toxin (sub)family, which after sequencing revealed over 100 unique V_HH clones. Sequences of the lead V_HHs and CDR3 of hit V_HHs are provided in Supplementary Table 4. We speculate that the discovery of multiple high-affinity, cross-reactive V_HHs may have been facilitated by our immunization strategy, which involved multiple venoms with a broad range of similar and dissimilar toxins (antigens). After our screening campaign, we further evaluated the top 21 unique cross-reactive V_HHs against their corresponding toxin family in a dose-response DELFIA, yielding EC_{50} values (half maximal effective concentrations) ranging from 1-15 nM (Fig. 2b). Subsequently, we selected the top 15 V_HHs, based on broad cross-reactivity and low EC_{50} values, and evaluated their binding kinetics using biolayer interferometry (BLI). All of the 15 tested cross-reactive V_HHs displayed low nanomolar affinity (K_D) with slow dissociation rates (k_{off} $<5.5\times10^{-4}$ s^{-1}) for most of their target toxins (Fig. 2c, Supplementary Fig. 3, and Supplementary Table 5).

Next, we evaluated the ability of these V_HHs to neutralize their target toxins *in vitro*. lNTx and sNTx exert their function by binding to the nicotinic acetylcholine receptors (nAChRs) at neuromuscular junctions, preventing acetylcholine binding and ion influx, which disrupts nerve-muscle communication and often results in paralysis (Fig. 1c).[36] To address the

neutralization of lNTx and sNTx, we measured nAChR currents in a human rhabdomyosarcoma cell line in patch-clamp assays[37] and observed that pre-incubation of anti-lNTx (a-lNTx) V_HHs with lNTx-3, lNTx-5, and lNTx-7 or anti-sNTx V_HHs with sNTx-1, sNTx-3, and sNTx-6 before addition to the cells protected the nAChR-mediated current, i.e. showing complete inhibition of neurotoxicity down to a 1:1 molar ratio between V_HH and toxin (Fig. 3a).

Besides neurotoxicity, envenoming from 8 of the 18 elapid snakes included in this study, 7 *Afronaja* and 1 *Hemachatus*, can cause severe local tissue damage. This is primarily due to the toxic actions of CTx and PLA_2 present in their venoms, acting either alone or synergistically (Fig. 1c).[38,39] We therefore assessed the ability of the discovered anti-CTx V_HHs and an anti-PLA_2 V_HH to neutralize venom-induced cytotoxicity in cell-viability assays. Specifically, we pre-incubated venoms from the 8 snake species with 3 different V_HHs individually, V_HH1 a-CTx, V_HH4 a-CTx, and V_HH20 a-PLA_2, before addition to a keratinocyte cell line. Both anti-CTx V_HHs demonstrated broad neutralization, providing 75-95% and 50-85% protection, respectively, against the cytotoxic effects from the venoms of all 7 *Afronaja,* while V_HH20 a-PLA_2 showed almost no neutralization of any of the tested venoms (Fig. 3b). We observed no neutralization of *H. haemachatus* venom, which was in accordance with the binding data, where neither V_HH1 a-CTx nor V_HH4 a-CTx bound to CTx from this venom. Among the 18 elapid snakes studied, PLA_2 exhibit the highest enzymatic activity in *Afronaja*, moderate activity in *Boulengerina* and *Hemachatus*, and negligible activity in *Uraeus* and *Dendroaspis*.[30] Thus, we also assessed the neutralizing effect of V_HH20 a-PLA_2 in an enzymatic assay and observed complete inhibition of PLA_2 activity in the *Afronaja* venoms, but no neutralization of *H. haemachatus* venom (Fig. 3c).

Design of a recombinant antivenom based on oligoclonal V_HHs

After demonstrating *in vitro* neutralization of several medically important toxin (sub)families by multiple V_HHs, we performed a series of WHO-recommended murine pre-incubation experiments[40,41] to examine whether these neutralizing effects would translate to *in vivo* protection. We first determined the median lethal dose (LD_{50}) for venom fractions, toxins, and whole venoms when administered intravenously (i.v.) (Supplementary Table 6), whereafter venoms were pre-incubated with either single or multiple V_HHs and administered to mice, with survival monitored for 24 hours.

With the aim of having as few V_HHs as possible in the recombinant antivenom, we evaluated the most broadly-neutralizing V_HHs against each toxin (sub)family. We started with

neutralization of individual pure toxins or toxin fractions, then moved to simple whole venoms with a few different toxin (sub)families present, and finally evaluated the neutralization of more complex venoms. First, we evaluated the neutralization of sNTx-3 and lNTx-7 using V_HH5 a-sNTx and V_HH9 a-lNTx, respectively (Supplementary Fig. 4a-b, Supplementary Table 7); this resulted in the survival of all mice. Thereafter, we combined these 2 V_HHs and tested them on the venoms from *N. haje* and *N. melanoleuca,* species known to produce venoms rich in sNTx and lNTx. Pre-incubation of the venoms with these 2 V_HHs prevented lethality in all mice (Supplementary Fig. 4c-d, Supplementary Table 7). We then moved to the more complex venom of *D. viridis*, which contains sNTx and lNTx, as well as AgTx, and Og XI.[25] Pre-incubation of venom with a mixture of V_HH5 a-sNTx, V_HH9 a-lNTx, V_HH15 a-Og XI, and V_HH13 a-AgTx, protected all mice (Supplementary Fig. 4e, Supplementary Table 7), qualifying these 4 V_HHs for inclusion in the recombinant antivenom. Next, we also wanted to ensure the neutralization of black mamba venom (*D. polylepis*), which is rich in dendrotoxins from the KUN family but also contains sNTx and lNTx. We observed that adding V_HH17 a-KUN to the 4 V_HHs resulted in the survival of all mice when challenged with *D. polylepis* venom (Supplementary Fig. 4f, Supplementary Table 7). To evaluate the necessity of V_HH15 a-Og XI and V_HH13 a-AgTx, a mixture of V_HH5 a-sNTx, V_HH9 a-lNTx, and V_HH17 a-KUN was tested against *D. viridis* and *D. jamesoni* venom. While mice challenged with *D. viridis* venom all survived, they showed signs of lethargy, and only 2 mice survived after being challenged with *D. jamesoni* venom, illustrating that full neutralization is not achieved without V_HH15 a-Og XI and V_HH13 a-AgTx V_HHs (Supplementary Fig. 4g, Supplementary Table 7). Lastly, we evaluated the neutralization of PLA_2 and CTx using *N. nigricollis* venom and observed that a combination of V_HH20 a-PLA_2 and 2 anti-CTx V_HHs (V_HH1 a-CTx and V_HH4 a-CTx), which show different binding patterns to CTxs and therefore might provide broader neutralization than each of the anti-CTx V_HHs alone, protected all mice from lethal venom effects (Supplementary Fig. 4h, Supplementary Table 7). In total, we selected 8 lead V_HHs targeting 7 medically important toxin (sub)families and combined these into an experimental polyvalent recombinant antivenom.

To gain insights into the molecular basis of the broad neutralization of the 8 lead V_HHs, co-crystallization, cryo-EM, and *in silico* structural modelling predictions of the V_HHs in complex with 1 of their target toxins were used to determine their binding interactions. These experiments indicated that the V_HHs interact with residues that are predominantly conserved across the target toxins that they neutralize (Fig. 4, Supplementary Fig. 5a-c, 6a-c, 7),

and that the V_HH:sNTx and V_HH:lNTX interactions are similar to those previously reported.[13,17,42] Interestingly, it was observed that V_HH1 α-CTx was biparatopic, which may explain why this V_HH was better at neutralizing cell cytotoxicity than V_HH4 α-Ctx (Fig. 3b). To the best of our knowledge, such biparatopic behavior has not previously been reported and is worthy of further investigation.

The recombinant antivenom prevents lethality

To assess whether the recombinant antivenom (i.e., the defined mixture of 8 selected V_HHs) could neutralize venom-induced lethality caused by all of the 18 most medically relevant snakes in sub-Saharan Africa, we performed a series of pre-incubation experiments in mice.[40] In this set of experiments, we first determined the LD_{50} values for the whole venoms injected i.v. (Supplementary Table 6). Then, 3 LD_{50} values of the venoms were pre-incubated with the same dose of recombinant antivenom and administered i.v. to groups of 5 mice. The composition and dose of the recombinant antivenom was kept consistent across all venoms to simulate a real product being deployed in Africa, with the dose corresponding to at least a 1:10 molar ratio between each targeted toxin (sub)family and the respective V_HH (Supplementary Table 8). Survival and signs of envenoming were monitored over a 24-hour period post-injection. We observed that the recombinant antivenom prevented venom-induced lethality for all included species except *D. angusticeps* (Fig. 5a). No evident signs of envenoming were observed in mice that were administered recombinant antivenom pre-incubated with venoms from *D. jamesoni*, *H. haemachatus, N. ashei*, *N. katiensis, N. mossambica, N. nigricincta, N. nigricollis, N. nubiae*, *N. pallida, N. anchietae, N. haje, N. nivea,* and *N. senegalensis*. In mice injected with the recombinant antivenom pre-incubated with the venoms from *N. melanoleuca* and *D. viridis,* only minor signs of envenoming, including closed eyes and periods of lethargy interspersed with episodes of excessive grooming, were observed. For mice injected with recombinant antivenom pre-incubated with *N. annulifera* venom, similar signs of envenoming appeared after 15 hours. The venom from *D. polylepis* pre-incubated with the recombinant antivenom caused an initial state of severe lethargy, which disappeared after 1-2 minutes. We speculate that this rapid transient effect could be caused by small molecules in the venom such as adenosine or acetylcholine, which the recombinant antivenom is not designed to neutralize.[43] For *D. angusticeps* venom, we observed that the recombinant antivenom prolonged the survival of mice to between 3 and 6 hours. This venom is rich in muscarinic toxins, fasciculins, and synergistically-acting toxins,[44] and we speculate that the synergy between these toxins, which

are not targeted by the recombinant antivenom, could be responsible for the observed delayed lethality.

To better evaluate the efficacy of the recombinant antivenom in a scenario mimicking real snakebite envenoming, we further performed rescue experiments using 11 venoms from 4 different (sub)genera.[11,45,46] To perform these experiments, we first determined the subcutaneous (s.c.) venom LD_{50} values. However, when attempting to determine s.c. LD_{50} values for *Afronaja* venoms, we observed severe muscle and skin damage at the injection sites, and mice were sacrificed due to ethical considerations. Given that local tissue damage is the most clinically relevant effect of *Afronaja* envenomings, we deemed rescue-from-lethality experiments for these species ethically unjustifiable. For the remaining 11 species, we administered 3 LD_{50} values of the venom subcutaneously (s.c.) (Supplementary Table 6), followed by i.v. administration of the recombinant antivenom 5 minutes later and monitored survival and signs of envenoming over a 24-hour period post-injection (Supplementary Table 9). In these rescue experiments, the dose of the recombinant antivenom was increased compared to the pre-incubation experiments relative to the increase in LD_{50} values that was observed when switching from i.v. to s.c. administration of venom (Supplementary Table 9). For comparison, the commercial Inoserp PAN-AFRICA antivenom was included at a dose recommended by the manufacturer to neutralize 3 LD_{50} values of venom. We observed that the recombinant antivenom completely prevented lethality induced by the venoms from *N. haje, N. annulifera, N. nivea, N. senegalensis, N. nubiae,* and *H. haemachatus* (Fig. 5b, Supplementary Table 9), and the mice showed no signs of envenoming. Furthermore, the recombinant antivenom also prevented lethality induced by the venom of *D. viridis* (Fig. 5b, Supplementary Table 9), although we observed signs of envenoming, including limited movement approximately 4 hours after venom injection and continuing throughout the experiment. In addition, after 20 hours, 4 out of 5 mice developed swelling and haemorrhage of the eyeballs, and 1 mouse developed an increased abdominal volume. For *N. melanoleuca* venom, partial neutralization was observed, with 3 out of 5 mice surviving and the time of death substantially extended for the other 2 mice (Fig. 5b, Supplementary Table 9). The surviving mice presented similar signs of envenoming as observed for *D. viridis*, but did not show an increased abdominal volume. Finally, for *D. polylepis* venom, the recombinant antivenom delayed the time of death from approximately 0.5 hour in the venom-only control mice to 2 hours, for *D. jamesoni* the time of death was delayed from approximately 30 min to 60 min and no protective effect was seen with the venom from *D. angusticeps* (Fig. 5b, Supplementary Table 9). Based on the difference between pre-incubation and rescue

experiments for *D. polylepis* and *D. jamesoni*, we hypothesize that this is due to the complex interplay between venom and antivenom pharmacokinetics. It has been observed that the ability of antivenoms to redistribute and neutralize the toxins once they have reached their target strongly depends on the affinity of the antibodies present in the antivenom for the toxin as well as the affinity of the toxin for its respective target within the tissue.[47] Furthermore, a delayed release of the toxins from the subcutaneous injection site, due to the so-called "depot effect", could occur after the V_HHs have been cleared from the circulation, which could have resulted in a recurrence of envenoming signs in the absence of repeated therapeutic dosing.[48-50] Notably, in the rescue setting, the Inoserp PAN-AFRICA antivenom showed only partial neutralization of all of the tested venoms and an extension of time of death for the venom from *N. melanoleuca*, demonstrating that, except for *D. polylepis*, the recombinant antivenom performed better than the commercial antivenom on all included venoms at the tested doses (Fig. 5b, Supplementary Table 9).

The recombinant antivenom prevents dermonecrosis

Current plasma-derived antivenoms are typically poor at preventing local tissue damage, resulting in a high morbidity rate, including limbs lost, in snakebite victims.[7-9] In elapid snakes in sub-Saharan Africa, local tissue damage is primarily associated with spitting snake species (i.e. *Afronaja* and *Hemachatus* spp.), and CTx and PLA_2 play the most important role.[39] We therefore next examined the ability of our 2 anti-CTx V_HHs (V_HH1 a-CTx and V_HH4 a-CTx) and anti-PLA_2 V_HH (V_HH20 a-PLA_2) to prevent venom-induced dermonecrosis caused by *N. mossambica*, *N. nigricollis,* and *H. haemachatus* using an *in vivo* pre-incubation setup. We mixed the 3 V_HHs and pre-incubated this mixture with each of the venoms before intradermal (i.d.) injection and measured the lesion size after 72 hours. The V_HH mixture significantly reduced the dermonecrotic lesion areas, and all but 1 mouse per treatment group showed a complete absence of lesion for the 2 *Naja* venoms (Fig. 5c). We then moved to a rescue setup, where the V_HH mixture was delivered i.d. to the same injection region 15 minutes after the venom. Despite observations of rapid discoloration at the injection site within the 15-minute treatment window, the V_HH mixture significantly reduced the size of the dermonecrotic lesions caused by each of the 3 venoms (Fig. 5c, Supplementary Fig. 8a).

After demonstrating the efficacy of the mixture of V_HH1 a-CTx, V_HH4 a-CTx, and V_HH20 a-PLA_2 in both pre-incubation and rescue setups, we evaluated the recombinant antivenom (containing the 8 V_HHs) in another rescue assay where the recombinant antivenom was delivered i.v. 15 minutes after i.d. injection of the venom. Inoserp PAN-AFRICA antivenom

was included for comparison with *N. nigricollis* venom at a dose recommended by the manufacturer to neutralize 3 LD_{50} values of venom. The recombinant antivenom reduced the size of the lesions caused by each of the 3 venoms at the 48-hour experimental endpoint, although these results were only statistically significant for *N. nigricollis* (Fig. 5d, Supplementary Fig. 8b). In comparison, we observed less, and statistically insignificant, reduction of lesion size for Inoserp PAN-AFRICA antivenom on the tested venom from *N. nigricollis* (Fig. 5d), demonstrating that the recombinant antivenom performs better than the existing treatment in this model at the tested doses.

Discussion

Previous studies have shown that broadly neutralizing antibodies or V_HHs against snake toxins can be discovered using phage or yeast display technology.[11,13,18,20,35,42,46,51-53] However, while these studies demonstrated that rodents challenged with venoms dominated by neurotoxins can be rescued using such antibodies[13,18] and V_HHs[20], they represent only an initial proof of principle when viewed from a product development or clinical perspective. Notably, all neutralized venoms have been dominated by only 1 or 2 toxin families, and all but 3 studies[17,18,20] have reported the use of only a single monoclonal antibody or V_HH to neutralize a whole venom. In this study, we take an exciting departure beyond earlier work and demonstrate how the first experimental polyvalent recombinant antivenom can be developed using as few as 8 V_HHs targeting toxins from 7 different protein (sub)families to achieve continent-wide elapid species coverage. We demonstrate its *in vivo* efficacy on 18 elapid venoms using the WHO recommended pre-incubation model and further confirm the efficacy on 11 of the venoms in a more challenging rescue model, which more closely mimics a real snakebite scenario.[45] Furthermore, at the tested doses, this experimental recombinant antivenom performs better than the commercial plasma-derived antivenom, Inoserp PAN-AFRICA, in preventing both dermonecrosis and lethality across all snake species tested, apart from *D. polylepis.* By showing that an efficacious polyvalent recombinant antivenom with unprecedented broad species coverage can be constructed using only 8 V_HHs, we challenge the common belief that only polyclonal antibodies can overcome and neutralize the complexity of snake venoms. Thereby, we answer the long-standing and important question in toxinology of how few antibodies are sufficient to develop a recombinant antivenom with clinical utility. Our work thus solidifies our previous working hypotheses that it is indeed possible to unravel the challenging complexity of venoms through proteomic analysis[30] and identify which toxins are sufficient to neutralize in order to develop effective antivenom products.[29,54,55]

In addition to mortality, we demonstrate the efficacy of the experimental recombinant antivenom in reducing dermonecrosis caused by the venoms of the spitting elapid snakes, *N. nigricollis*, *N. mossambica*, and *H. haemachatus*, both in a pre-incubation and 2 rescue models. Although plasma-derived antivenoms have demonstrated efficacy in pre-incubation models of dermonecrosis, they have rarely been assessed in rescue models.[56] Further, it is well established that antivenoms are largely ineffective in preventing severe local tissue damage unless given rapidly after a bite[56,57], which is typically attributed to the limited ability of whole IgGs or IgG fragments administered i.v. to penetrate deep tissue and the speed with which local tissue damage develops. In comparison, we here show that delayed local administration (i.d.) of toxin-specific V_HHs significantly reduces dermonecrosis caused by different elapid snake venoms, analogous to recent findings with the PLA_2-inhibiting small molecule, varespladib, and the CTx-inhibiting heparinoid, tinzaparin.[58,59] In addition, the recombinant antivenom further provides significant protection against dermonecrosis caused by *N. nigricollis* venom in a rescue model when administered i.v. This finding is particularly promising given the rapid onset of toxicity caused by locally acting toxins that induce tissue damage, the ineffectiveness of current antivenoms (i.e. Fig. 5d), and the lack of protection previously offered by intravenous varespladib[58]. Interestingly, neither the V_HH20 a-PLA_2, V_HH1 a-CTx, nor V_HH4 a-CTx neutralizes the *H. haemachatus* venom *in vitro* in the cell viability or phospholipase activity assays. These findings highlight the need for further investigation to elucidate the mechanisms underlying the observed neutralization of local tissue damage in mouse experiments.

Regarding design features for our experimental recombinant antivenom, we chose to employ the V_HH format, as this simple antibody format could provide a recombinant antivenom with several advantages. First of all, the use of this clinically proven antibody format might aid in the development of a safe product with a low risk of causing severe immunological reactions upon administration due to the typically low immunogenicity observed for V_HHs.[4] An enhanced safety profile may enable earlier treatment of patients by removing the need to wait for clinical syndromes to manifest before administration of antivenom. Second, V_HHs are known to have a remarkably high biophysical stability, which is likely to translate into a long shelf-life that might be advantageous for products that may need to be stockpiled for longer periods, possibly in humid or high-temperature conditions. Third, the small size of V_HHs enables them to rapidly distribute from the bloodstream into the surrounding tissues and thereby neutralize toxins at the bite site or site of action. Finally, the small size of V_HHs compared to full-length IgGs provides them with a large neutralization capacity per mass of

antivenom.[60] Combined with the possibility of manufacturing V_HHs using low-cost microbial expression systems, this might facilitate a lower cost of goods for treatment. In turn, a lower cost of goods could positively impact affordability and make antivenoms more accessible to people in low and middle-income countries who disproportionally suffer the greatest burden of snakebite.[61]

Despite these advantages, recombinant V_HHs are also associated with certain limitations. Most importantly, the short half-life of V_HHs in circulation could potentially limit their sustained action over time, which could prove to be problematic, as snake toxins may exit the bite site and enter circulation long after the snakebite incident due to "depot effect".[48-50] However, it is also possible that the ability of V_HHs to rapidly penetrate into deep tissue could counter this effect, as it might allow the V_HHs to neutralize the toxins before they are released into circulation. To study this complex interplay between pharmacodynamics of the V_HHs and the toxicokinetics of the venom components, large animal experiments are likely required. If it is found necessary, repeated pharmacokinetic-informed dosing can be applied or the half-life of the V_HHs could possibly be extended through various antibody engineering techniques, such as multimerization or linking them to a human IgG Fc-domain.[20,51] Finally, it is possible that our cocktail could be further simplified by reducing the number of molecules included, which would likely be beneficial from a manufacturing perspective. This could either be achieved by improving the broadly-neutralizing capacity of some of our V_HHs, such as those targeting CTx, and including only 1 broadly-neutralizing V_HH per toxin subfamily. Moreover, engineering heterodivalent/trivalent V_HH constructs,[62,63] through fusion of 2-3 V_HHs could reduce the number of individual molecules required to neutralize the described toxin specificities, which could further simplify manufacturing. However, the total amount of material needed in terms of weight would remain the same (or become higher), and we speculate that the favourable deep tissue penetrating properties of the small monomeric V_HHs risk being compromised, based on what is known from the oncology field.[64] Nevertheless, further refinement of the cocktail is likely possible and should be further investigated alongside the development of a manufacturing strategy and an assessment of whether the V_HHs might be useful for neutralizing venoms from related Asian elapids.

While the work here focused on developing a defined oligoclonal mixture of V_HHs against African elapid venoms, the strategy employed for antibody discovery and therapeutic prototype design holds promise for broader applications. Specifically, it may be valuable in clinical contexts where targeting multiple isoforms across both closely and distantly related protein families is essential. We speculate that, beyond other animal envenomings, the approaches

described here could be useful for the development of advanced therapies against infectious diseases or complex immunological or endocrinological disorders.

Acknowledgement

The authors thank Emelie Riis for her help during the phage display selection rounds, Marie Vestergaard Lukassen and Maike Nielsen for help during the mass spectrometry experiments, and Suzana Siebenhaar for help during protein crystal screening.

Mass spectrometry analysis was performed at the DTU Proteomics Core, Technical University of Denmark, supported by PRO-MS: Danish National Mass Spectrometry Platform for Functional Proteomics [5072-00007B]. The V_HH expression vector was a kind gift from the laboratory of Professor Bart De Strooper at the KU Leuven and VIB. BioRender was used to create figures. The authors acknowledge the use of the Biomedical Services Unit provided by Liverpool Shared Research Facilities, Faculty of Health and Life Sciences, University of Liverpool, UK. We acknowledge the MAX IV Laboratory for beamtime on the Beamline Biomax [20240265]. Research conducted at MAX IV, a Swedish national user facility, is supported by Vetenskapsrådet [2018-07152], Vinnova [2018-04969], and Formas [2019-02496].

K.K. is supported by a grant from the Novo Nordisk Foundation [NNF16OC0020670]. A.H.L. is supported by a grant from the European Research Council (ERC) under the European Union's Horizon 2020 research and innovation program [850974], a grant from the Villum Foundation [00025302], and a grant from Wellcome [221702/Z/20/Z]. M.B.V. is supported by a Eurotech Postdoctoral fellowship from the European Union's Horizon 2020 research and innovation program under the Marie Skłodowska-Curie grant agreement [899987]. A.A. has received funding from the Mexican Consejo Nacional de Ciencia y Tecnología, FORDECyT-PRONAII [303045]. N.R.C. is supported by grants from Wellcome [221708/Z/20/Z and 223619/Z/21/Z]. S.T. is supported by a scholarship from the Anandamahidol Foundation under the Royal Patronage of His Majesty King Bhumibol Adulyadej of Thailand. T.P.J. is supported from the Alliance programme under the EuroTech Universities agreement, as well as under the Marie Sklodowska-Curie grant [713683] (COFUNDfellowsDTU). St.A. is supported by a grant UK Research and Innovation [MR/S03398X/1] and NC3Rs [NC/X001172/1]. S.P.M. is supported by a grant from the National Science Foundation [IOS-2307044]. J.P.M. is supported by a grant from the Novo Nordisk Foundation [NNF24OC0088714].

Author contributions

Conceptualization: T.P.J., A.L., A.H.L.

Methodology: Sh.A., N.J.B., M.B.V., A.L., A.H.L.

Investigation: Sh.A., N.J.B., M.B.V., A.G.M., S.K., I.A.C., A.E.M., R.J.E., E.C., E.N.C., M.L.F.Q., G.T.T.N., C.O.B., Y.W., K.K., S.T., T.W.E., C.H.D., E.U.G.S., T.J., K.B., E.M., E.R.T.,J.P.M.,S.K.M., N.R.C.

Visualization: Sh.A., N.J.B., M.B.V.

Funding acquisition: M.B.V., K.K., J.P.M, A.A., S.P.M., St.A., N.R.C., T.P.J, A.H.L.Project administration: A.L., A.H.L.

Resources: A.B.W., A.A., S.P.M., St.A., N.R.C., A.H.L.

Supervision: A.L., A.H.L.

Writing – original draft: Sh.A., N.J.B., M.B.V., T.P.J., A.L., A.H.L.

Writing – review & editing: Sh.A., N.J.B., M.B.V., A.G.M., S.K., I.A.C., A.E.M, R.J.E., E.C., E.N.C, M.L.F.Q., G.T.T.N., C.O.B., Y.W., K.K., S.T., T.W.E., C.H.D., E.U.G.S., T.J., K.B., E.M., E.R.T., A.B.W., J.P.M., A.A., S.P.M., St.A., S.K.M., N.R.C., T.P.J., A.L., A.H.L.

Corresponding authors: T.P.J., A.L., A.H.L.

Ethics declarations

The authors declare no conflicts of interest.

For systemic envenoming experiments, all animals and *in* vivo methodologies used were approved by the bioethics committee of the Institute of Biotechnology, Universidad Nacional Autónoma de México (IBt-UNAM) under project 481 or the University of Northern Colorado Institutional Animal Care and Use Committee (UNC-IACUC), the Department of Biological Sciences under project 2208D-SM-SMLBirds. For dermonecrosis experiments, ethical approvals were obtained from the Animal Welfare and Ethics Review Boards of Liverpool School of Tropical Medicine and The University of Liverpool, and work was performed under UK Home Office Project Licences P58464F90 and PP2669304 in accordance with the UK Animal (Scientific Procedures) Act 1986.

References

1 Chippaux, J.-P. Estimate of the burden of snakebites in sub-Saharan Africa: A meta-analytic approach. *Toxicon* **57**, 586-599, doi.org/10.1016/j.toxicon.2010.12.022 (2011).

2 Alcoba, G. *et al.* Snakebite Epidemiology in Humans and Domestic Animals in Rural Cameroon: A Nationwide Random Multi-Cluster Community Survey. *SSRN*, doi:10.2139/ssrn.4867534 (2024).

3 Kini, R. M., Sidhu, S. S. & Laustsen, A. H. Biosynthetic Oligoclonal Antivenom (BOA) for Snakebite and Next-Generation Treatments for Snakebite Victims. *Toxins* **10**, doi:10.3390/toxins10120534 (2018).

4 Thumtecho, S., Burlet, N. J., Ljungars, A. & Laustsen, A. H. Towards better antivenoms: navigating the road to new types of snakebite envenoming therapies. *The journal of venomous animals and toxins including tropical diseases* **29**, e20230057, doi:10.1590/1678-9199-jvatitd-2023-0057 (2023).

5 Guadarrama-Martínez, A., Neri-Castro, E., Boyer, L. & Alagón, A. Variability in antivenom neutralization of Mexican viperid snake venoms. *PLOS Neglected Tropical Diseases* **18**, e0012152, doi:10.1371/journal.pntd.0012152 (2024).

6 Segura, Á. *et al.* Assessment of snake antivenom purity by comparing physicochemical and immunochemical methods. *Biologicals* **41**, 93-97, doi.org/10.1016/j.biologicals.2012.11.001 (2013).

7 Silva, A. & Isbister, G. K. Current research into snake antivenoms, their mechanisms of action and applications. *Biochemical Society transactions* **48**, 537-546, doi:10.1042/bst20190739 (2020).

8 Lalloo, D. G. & Theakston, R. D. G. Snake Antivenoms. *Journal of Toxicology: Clinical Toxicology* **41**, 277-290, doi:10.1081/CLT-120021113 (2003).

9 Alangode, A., Rajan, K. & Nair, B. G. Snake antivenom: Challenges and alternate approaches. *Biochemical Pharmacology* **181**, 114135, doi.org/10.1016/j.bcp.2020.114135 (2020).

10 Menzies, S. K., N., P. R. & and Ainsworth, S. Practical progress towards the development of recombinant antivenoms for snakebite envenoming. *Expert Opinion on Drug Discovery* **20**, 799-819, doi:10.1080/17460441.2025.2495943 (2025).

11 Ledsgaard, L. *et al.* Discovery and optimization of a broadly-neutralizing human monoclonal antibody against long-chain α-neurotoxins from snakes. *Nature Communications* **14**, 682, doi:10.1038/s41467-023-36393-4 (2023).

12 Sørensen, C. V. *et al.* Antibody-dependent enhancement of toxicity of myotoxin II from *Bothrops asper*. *Nature Communications* **15**, 173, doi:10.1038/s41467-023-42624-5 (2024).

13 Khalek, I. S. *et al.* Synthetic development of a broadly neutralizing antibody against snake venom long-chain α-neurotoxins. *Science translational medicine* **16**, eadk1867, doi:10.1126/scitranslmed.adk1867 (2024).

14 Danpaiboon, W. *et al. Ophiophagus hannah* Venom: Proteome, Components Bound by *Naja kaouthia* Antivenin and Neutralization by *N. kaouthia* Neurotoxin-Specific Human ScFv. *Toxins* **6**, 1526-1558 doi.org/10.3390/toxins6051526 (2014).

15 Prado, N. D. R. *et al.* Inhibition of the Myotoxicity Induced by *Bothrops jararacussu* Venom and Isolated Phospholipases A_2 by Specific Camelid Single-Domain Antibody Fragments. *PloS one* **11**, e0151363, doi:10.1371/journal.pone.0151363 (2016).

16 Kazemi-Lomedasht, F. *et al.* Development of a human scFv antibody targeting the lethal Iranian cobra (*Naja oxiana*) snake venom. *Toxicon* **171**, 78-85, doi.org/10.1016/j.toxicon.2019.10.006 (2019).

17 Glanville, J. *et al.* Snake venom protection by a cocktail of varespladib and broadly neutralizing human antibodies. *Cell* **188**, doi.org/10.1016/j.cell.2025.03.050 (2025).
18 Laustsen, A. H. *et al. In vivo* neutralization of dendrotoxin-mediated neurotoxicity of black mamba venom by oligoclonal human IgG antibodies. *Nature Communications* **9**, 3928, doi:10.1038/s41467-018-06086-4 (2018).
19 Silva, L. C. *et al.* Discovery of human scFvs that cross-neutralize the toxic effects of *B. jararacussu* and *C. d. terrificus* venoms. *Acta Tropica* **177**, 66-73, doi.org/10.1016/j.actatropica.2017.09.001 (2018).
20 Benard-Valle, M. *et al. In vivo* neutralization of coral snake venoms with an oligoclonal nanobody mixture in a murine challenge model. *Nature Communications* **15**, 4310, doi:10.1038/s41467-024-48539-z (2024).
21 Bailon Calderon, H. *et al.* Development of Nanobodies Against Hemorrhagic and Myotoxic Components of *Bothrops atrox* Snake Venom. *Frontiers in immunology* **11**, doi:10.3389/fimmu.2020.00655 (2020).
22 Cristina, R. T. *et al.* Protein structure of the venom in nine species of snake: from bio-compounds to possible healing agents. *Brazilian journal of medical and biological research* **53**, e9001, doi:10.1590/1414-431x20199001 (2020).
23 Casewell, N. R., Jackson, T. N. W., Laustsen, A. H. & Sunagar, K. Causes and Consequences of Snake Venom Variation. *Trends in Pharmacological Sciences* **41**, 570-581, doi.org/10.1016/j.tips.2020.05.006 (2020).
24 Smith, G. P. Filamentous Fusion Phage: Novel Expression Vectors That Display Cloned Antigens on the Virion Surface. *Science* **228**, 1315-1317, doi:10.1126/science.4001944 (1985).
25 McCafferty, J., Griffiths, A. D., Winter, G. & Chiswell, D. J. Phage antibodies: filamentous phage displaying antibody variable domains. *Nature* **348**, 552-554, doi:10.1038/348552a0 (1990).
26 Spawls, S. & Branch, B. *The dangerous snakes of Africa*. (Bloomsbury Publishing, 2020).
27 O'Shea, M. *Venomous snakes of the world*. (Princeton University Press, 2005).
28 Muller, G. J., Modler, H., Wium, C. A., Marks, C. J. & Veale, D. J. H. Snake bite in southern Africa : diagnosis and management. *CME* **30**, 362-382, doi:10.10520/EJC126922 (2012).
29 Laustsen, A. H. Guiding recombinant antivenom development by omics technologies. *New biotechnology* **45**, 19-27, doi:10.1016/j.nbt.2017.05.005 (2018).
30 Nguyen, G. T. T. *et al.* High-throughput proteomics and *in vitro* functional characterization of the 26 medically most important elapids and vipers from sub-Saharan Africa. *GigaScience* **11**, doi:10.1093/gigascience/giac121 (2022).
31 Hiremath, K. *et al.* Three finger toxins of elapids: structure, function, clinical applications and its inhibitors. *Molecular Diversity* **28**, doi:10.1007/s11030-023-10734-3 (2023).
32 Kini, R. M. & Doley, R. Structure, function and evolution of three-finger toxins: Mini proteins with multiple targets. *Toxicon* **56**, 855-867, doi.org/10.1016/j.toxicon.2010.07.010 (2010).
33 Ainsworth, S. *et al.* The medical threat of mamba envenoming in sub-Saharan Africa revealed by genus-wide analysis of venom composition, toxicity and antivenomics profiling of available antivenoms. *Journal of proteomics* **172**, 173-189, doi:10.1016/j.jprot.2017.08.016 (2018).
34 Sørensen, C. V. *et al.* Cross-reactivity trends when selecting scFv antibodies against snake toxins using a phage display-based cross-panning strategy. *Scientific Reports* **13**, 10181, doi:10.1038/s41598-023-37056-6 (2023).

35 Ahmadi, S. *et al.* An *in vitro* methodology for discovering broadly-neutralizing monoclonal antibodies. *Scientific Reports* **10**, 10765, doi:10.1038/s41598-020-67654-7 (2020).

36 Nirthanan, S. Snake three-finger α-neurotoxins and nicotinic acetylcholine receptors: molecules, mechanisms and medicine. *Biochemical Pharmacology* **181**, 114168, doi.org/10.1016/j.bcp.2020.114168 (2020).

37 Ahmadi, S. *et al.* From squid giant axon to automated patch-clamp: electrophysiology in venom and antivenom research. *Frontiers in pharmacology* **14**, doi:10.3389/fphar.2023.1249336 (2023).

38 Pucca, M. B. *et al.* Unity Makes Strength: Exploring Intraspecies and Interspecies Toxin Synergism between Phospholipases A_2 and Cytotoxins. *Frontiers in pharmacology* **11**, 611, doi:10.3389/fphar.2020.00611 (2020).

39 Petras, D. *et al.* Snake venomics of African spitting cobras: toxin composition and assessment of congeneric cross-reactivity of the pan-African EchiTAb-Plus-ICP antivenom by antivenomics and neutralization approaches. *Journal of proteome research* **10**, 1266-1280, doi:10.1021/pr101040f (2011).

40 Gutiérrez, J. M. *et al. In Vitro* Tests for Assessing the Neutralizing Ability of Snake Antivenoms: Toward the 3Rs Principles. *Frontiers in immunology* **11**, 617429, doi:10.3389/fimmu.2020.617429 (2020).

41 Guidelines for the production, control and regulation of snake antivenom immunoglobulins, Annex 5, TRS No 1004. 192 (World Health Organisation, 2013).

42 Damsbo, A. *et al.* Structural mechanisms behind the neutralisation of long-chain α-neurotoxins by broadly neutralising V_HHs discovered using a consensus antigen. *Communications Chemistry* **8**, 209, doi:10.1038/s42004-025-01600-4 (2025).

43 Villar-Briones, A. & Aird, S. D. Organic and Peptidyl Constituents of Snake Venoms: The Picture Is Vastly More Complex Than We Imagined. *Toxins* **10**, doi:10.3390/toxins10100392 (2018).

44 Lauridsen, L. P., Laustsen, A. H., Lomonte, B. & Gutiérrez, J. M. Toxicovenomics and antivenom profiling of the Eastern green mamba snake (*Dendroaspis angusticeps*). *Journal of proteomics* **136**, 248-261, doi.org/10.1016/j.jprot.2016.02.003 (2016).

45 Knudsen, C. *et al.* Novel Snakebite Therapeutics Must Be Tested in Appropriate Rescue Models to Robustly Assess Their Preclinical Efficacy. *Toxins* **12,** doi.org/10.3390/toxins12090528 (2020).

46 Ledsgaard, L. *et al. In vitro* discovery of a human monoclonal antibody that neutralizes lethality of cobra snake venom. *mAbs* **14**, 2085536, doi:10.1080/19420862.2022.2085536 (2022).

47 Gutiérrez, J. M., León, G. & Lomonte, B. Pharmacokinetic-Pharmacodynamic Relationships of Immunoglobulin Therapy for Envenomation. *Clinical Pharmacokinetics* **42**, 721-741, doi:10.2165/00003088-200342080-00002 (2003).

48 Paniagua, D., Vergara, I., Boyer, L. & Alagón, A. in *Snake Venoms* (eds Hidetoshi Inagaki *et al.*) 453-474 (Springer Netherlands, 2017).

49 Seifert, S. A. & Boyer, L. V. Recurrence phenomena after immunoglobulin therapy for snake envenomations: Part 1. Pharmacokinetics and pharmacodynamics of immunoglobulin antivenoms and related antibodies. *Annals of emergency medicine* **37**, 189-195, doi:10.1067/mem.2001.113135 (2001).

50 Paniagua, D. *et al.* Antivenom effect on lymphatic absorption and pharmacokinetics of coral snake venom using a large animal model. *Clinical Toxicology* **57**, 727-734, doi:10.1080/15563650.2018.1550199 (2019).

51 Richard, G. *et al. In vivo* neutralization of α-cobratoxin with high-affinity llama single-domain antibodies (V_HHs) and a V_HH-Fc antibody. *PloS one* **8**, e69495, doi:10.1371/journal.pone.0069495 (2013).

52 Sørensen, C. V. *et al.* Discovery of a human monoclonal antibody that cross-neutralizes venom phospholipase A_2s from three different snake genera. *Toxicon* **234**, 107307, doi.org/10.1016/j.toxicon.2023.107307 (2023).

53 Damsbo, A. *et al.* Discovery of broadly neutralizing V_HHs against short-chain α-neurotoxins using a consensus toxin as an antigen. *mAbs* **17**, 2522838, doi:10.1080/19420862.2025.2522838 (2025).

54 Laustsen, A. H. Toxin-centric development approach for next-generation antivenoms. *Toxicon* **150**, 195-197, doi:10.1016/j.toxicon.2018.05.021 (2018).

55 Laustsen, A. H., Lohse, B., Lomonte, B., Engmark, M. & Gutiérrez, J. M. Selecting key toxins for focused development of elapid snake antivenoms and inhibitors guided by a Toxicity Score. *Toxicon* **104**, 43-45, doi:10.1016/j.toxicon.2015.07.334 (2015).

56 Rivel, M. *et al.* Pathogenesis of dermonecrosis induced by venom of the spitting cobra, *Naja nigricollis*: An experimental study in mice. *Toxicon* **119**, 171-179, doi.org/10.1016/j.toxicon.2016.06.006 (2016).

57 Lin, C.-C., Chaou, C.-H. & Gao, S.-Y. Influential Factors of Local Tissue Necrosis after Taiwan Cobra Bites: A Secondary Analysis of the Clinical Significance of Venom Detection in Patients of Cobra Snakebites. *Toxins* **13**, doi.org/10.3390/toxins13050338 (2021).

58 Bartlett, K. E. *et al.* Dermonecrosis caused by a spitting cobra snakebite results from toxin potentiation and is prevented by the repurposed drug varespladib. *Proceedings of the National Academy of Sciences* **121**, e2315597121, doi:10.1073/pnas.2315597121 (2024).

59 Du, T. Y. *et al.* Molecular dissection of cobra venom highlights heparinoids as an antidote for spitting cobra envenoming. *Science translational medicine* **16**, eadk4802, doi:10.1126/scitranslmed.adk4802 (2024).

60 Ljungars, A. & Laustsen, A. H. Neutralization capacity of recombinant antivenoms based on monoclonal antibodies and nanobodies. *Toxicon* **222**, 106991, doi.org/10.1016/j.toxicon.2022.106991 (2023).

61 Jenkins, T. P. & Laustsen, A. H. Cost of Manufacturing for Recombinant Snakebite Antivenoms. *Frontiers in bioengineering and biotechnology* **8**, doi:10.3389/fbioe.2020.00703 (2020).

62 Rodriguez Rodriguez, E. R. *et al.* Fit-for-purpose heterodivalent single-domain antibody for gastrointestinal targeting of toxin B from *Clostridium difficile*. *Protein science* **33**, e5035, doi.org/10.1002/pro.5035 (2024).

63 Wade, J. *et al.* Generation of Multivalent Nanobody-Based Proteins with Improved Neutralization of Long α-Neurotoxins from Elapid Snakes. *Bioconjugate Chemistry* **33**, 1494-1504, doi:10.1021/acs.bioconjchem.2c00220 (2022).

64 Debie, P. *et al.* Size and affinity kinetics of nanobodies influence targeting and penetration of solid tumours. *Journal of Controlled Release* **317**, 34-42, doi.org/10.1016/j.jconrel.2019.11.014 (2020).

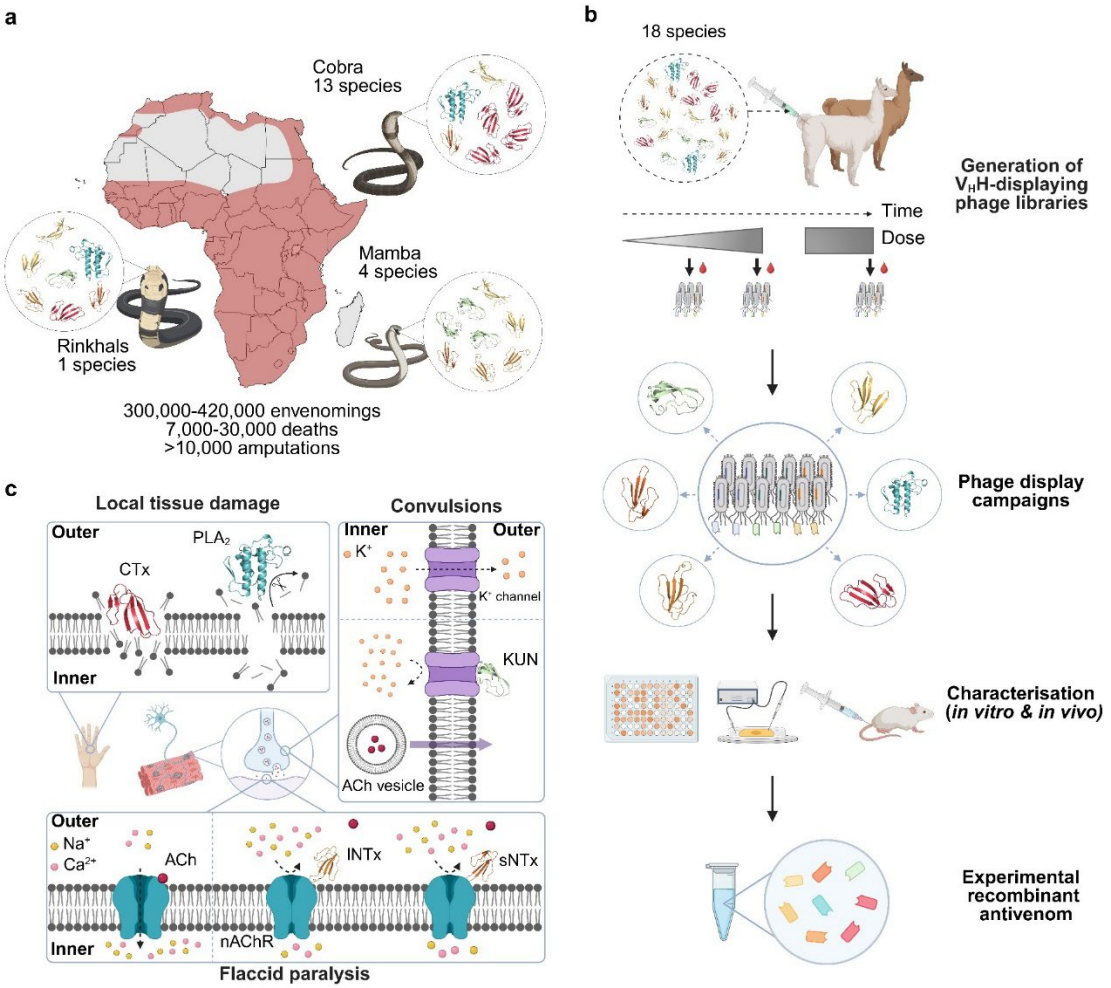

Fig. 1: Schematic overview of the study and the function of targeted toxin families. **a,** The distribution of the 18 most medically relevant elapid snakes from sub-Saharan Africa with the estimated snakebite envenoming incidence, fatality rate, and morbidity.[1,65] **b,** Schematic overview of the pipeline used for the development of the experimental recombinant antivenom. A pair of camelids were immunized with a mixture of whole venoms from 18 elapid snakes to generate immune V_HH-displaying phage libraries for discovery of V_HHs with broad cross-reactivity and high affinity. The V_HHs were characterized *in vitro* and *in vivo*, and 8 V_HHs were chosen and combined into an experimental recombinant antivenom. **c,** Visual representation of the pathology of the included major toxin families. A type IA cytotoxin[66] (CTx, dark red, PDB ID: 9BK6) disrupts lipid bilayers, and a phospholipase A_2[67] (PLA_2, cyan, PDB ID: 1A3D) catalyzes the hydrolysis of fatty acids from the phospholipids, both causing local tissue damage.[38,68,69] Both a type I α-neurotoxin[70] (sNTx, dark orange, PDB ID: 1VB0) and a type II α-neurotoxin[66] (lNTx, light orange, PDB ID: 9BK5) block acetylcholine (ACh) from binding to nicotinic acetylcholine receptors (nAChRs), preventing ion flux and leading to flaccid paralysis.[32] A Kunitz-type serine protease inhibitor[71] (KUN, light green, PDB ID: 1DEM) blocks voltage-gated K^+ channels, causing enhanced ACh release and subsequent convulsions.[72]

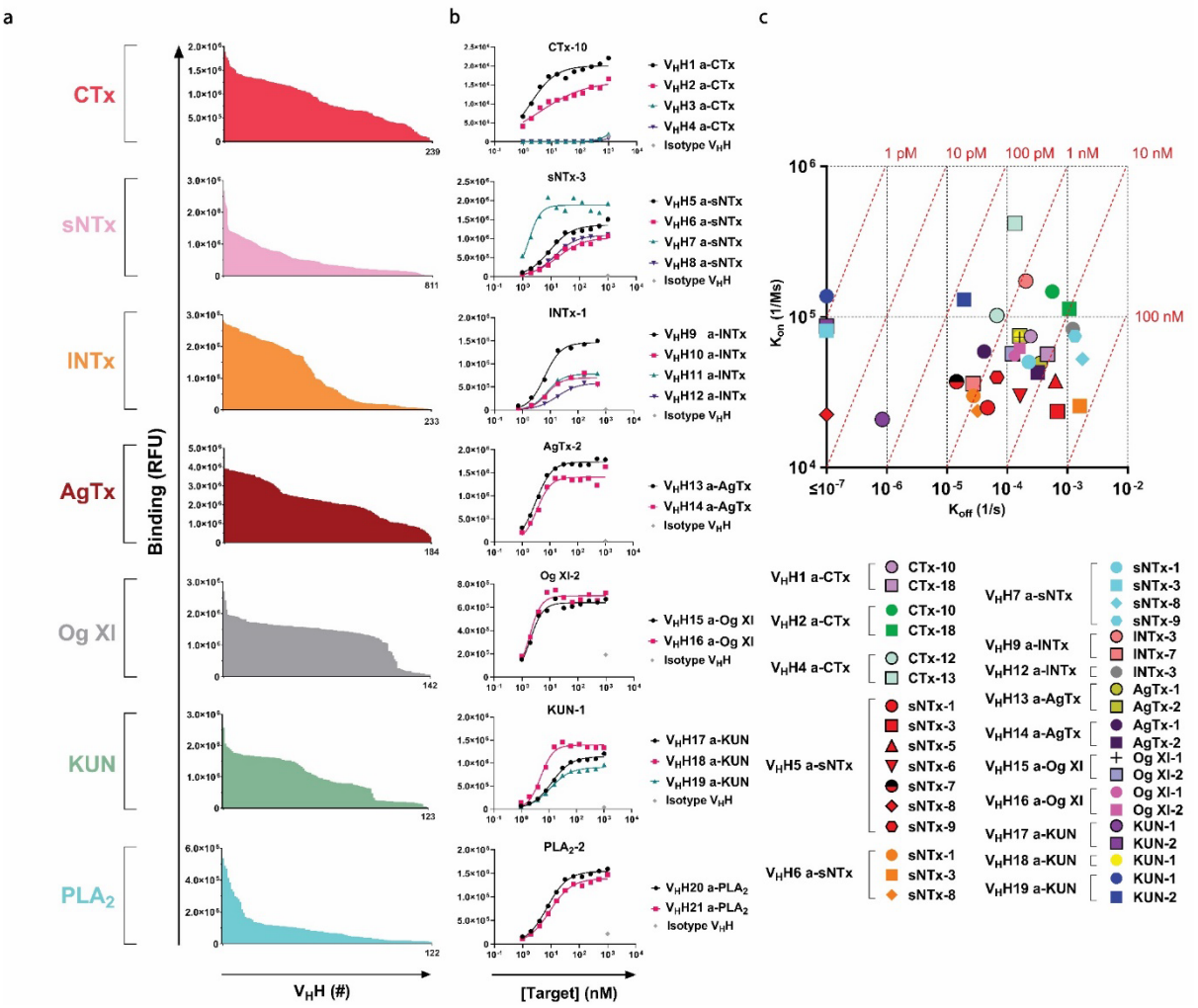

Fig. 2: Screening, dose-response binding curves, and isoaffinity plot of monoclonal V_HHs binding to toxins and venom fractions. **a,** Screening of over 3,000 V_HH clones for binding to their cognate toxin in an expression-normalized capture DELFIA. Only V_HHs with a signal intensity 10 times above the background level are shown, with the number of clones exceeding this threshold displayed on the x-axis. **b,** Dose-response binding curves for 21 V_HHs against a venom fraction or a toxin representing each targeted toxin (sub)family measured using an expression-normalized capture DELFIA. **c,** Isoaffinity plot of 15 cross-reactive V_HHs binding to venom fractions and toxins from various snake (sub)genera measured with biolayer interferometry. Due to the instrument's detection limit for dissociation rates (k_{off}) of 10^{-7} s^{-1}, 4 points below this cutoff are plotted at $\leq 10^{-7}$ s^{-1}. The red diagonal lines represent specific K_D values, which are labeled above each line.

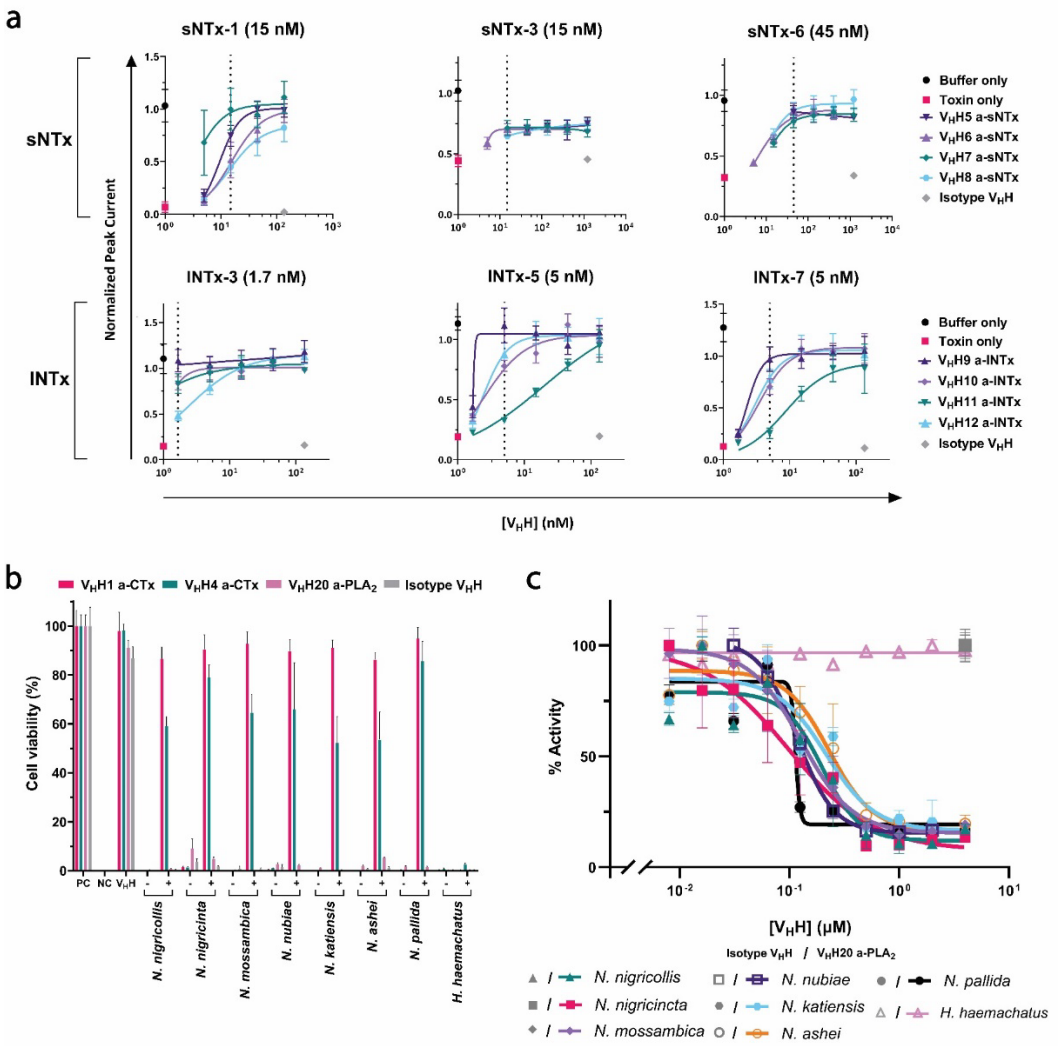

Fig. 3: *In vitro* neutralization of sNTx, lNTx, CTx, and PLA_2. **a,** Neutralization of sNTx- and lNTx-mediated blocking of the muscle-type nAChR current in whole-cell patch-clamp. Dose-response curves are shown with increasing concentrations of V_HH to prevent the blocking of nAChRs by sNTx-1, sNTx-3, sNTx-6, lNTx-3, lNTx-5, and lNTx-7. Experiments were performed using 8 replicates, and results are expressed as mean ± SD. The toxin concentrations are shown in parentheses, and the dotted line represents a 1:1 molar ratio of toxin:V_HH. **b,** Neutralization of venom-induced cytotoxicity using a cell viability assay with a N/TERT keratinocyte cell line. The positive control (PC) included media supplemented with PBS and was set to 100% cell viability. For the negative control (NC), media supplemented with triton X-100 was added, resulting in complete cell death. As an additional control, V_HH without any venom was included (V_HH). For all venoms, (-) indicates 2 IC_{50}s of the venom without V_HH addition, and (+) indicates venom incubated with a V_HH at a 1:5 molar ratio of CTx or PLA_2 to V_HH. Experiments were conducted in triplicate, and results are expressed as mean ± SD. **c,** Neutralization of PLA_2 enzymatic activity in the whole venoms of *H. haemachatus* and all *Afronaja* species by V_HH20 a-PLA_2 using a colorimetric enzymatic activity assay with the chromogenic substrate NOBA (4-nitro-3-(octanoyloxy)benzoic acid). Experiments were conducted in duplicates, and results are expressed as mean ± SD.

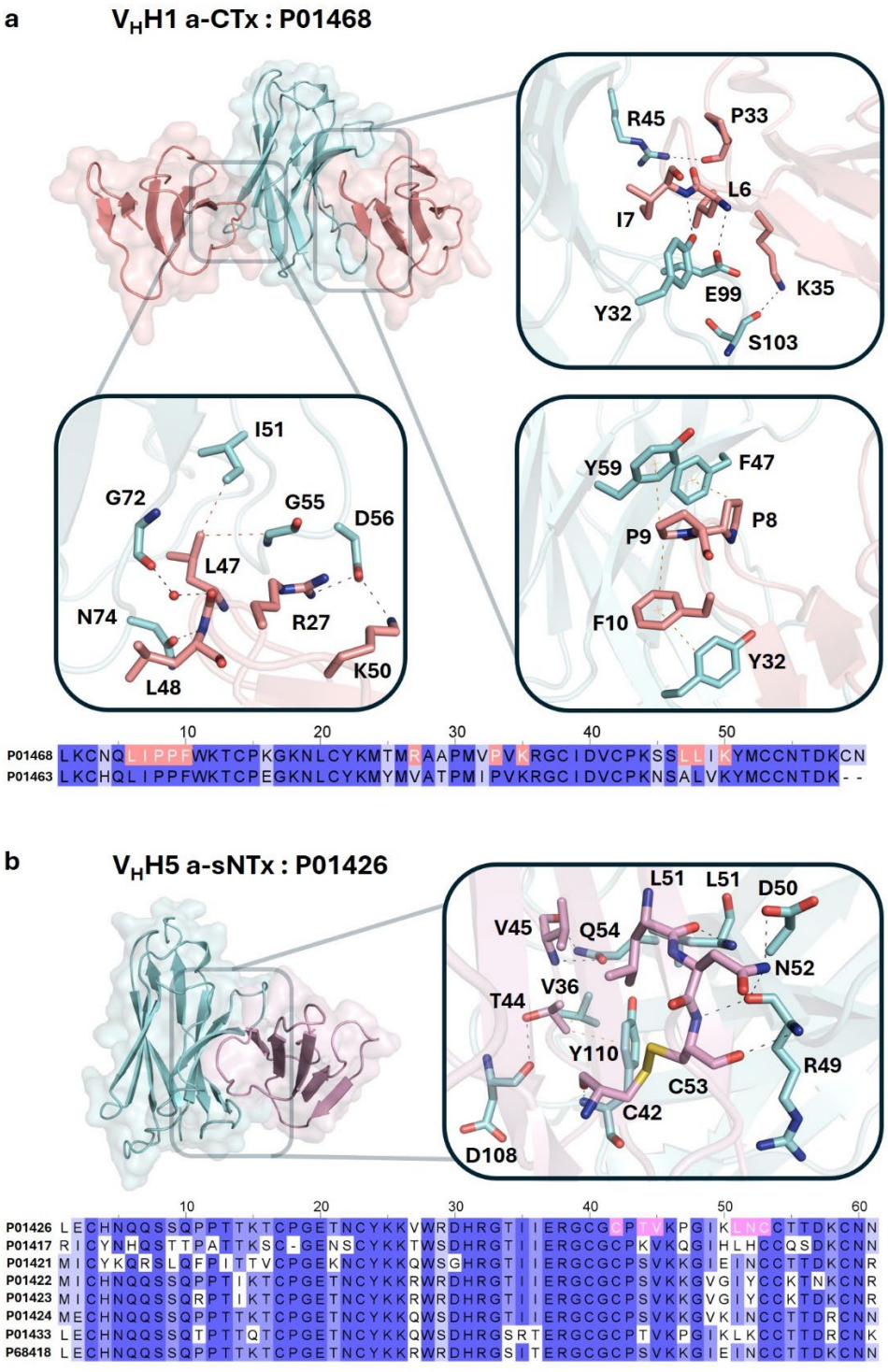

Fig. 4. Interactions in co-crystal structures of **a,** the biparatopic V_HH1 a-CTx (light blue) binding 2 different epitopes of cardiotoxin (P01468) (salmon) and **b,** V_HH5 a-sNTx (light blue) with short neurotoxin 1 (P01426) (purple). The close-ups illustrate the hydrogen bonds (black dotted lines), π-π and π-C_H bonds (orange dotted lines), and Van der Waals bonds (red dotted lines). Sequence alignments of the verified target toxins of each respective V_HH are shown under their structures. Here, the epitope residues of the target toxin present in the crystal structure are highlighted in corresponding colors.

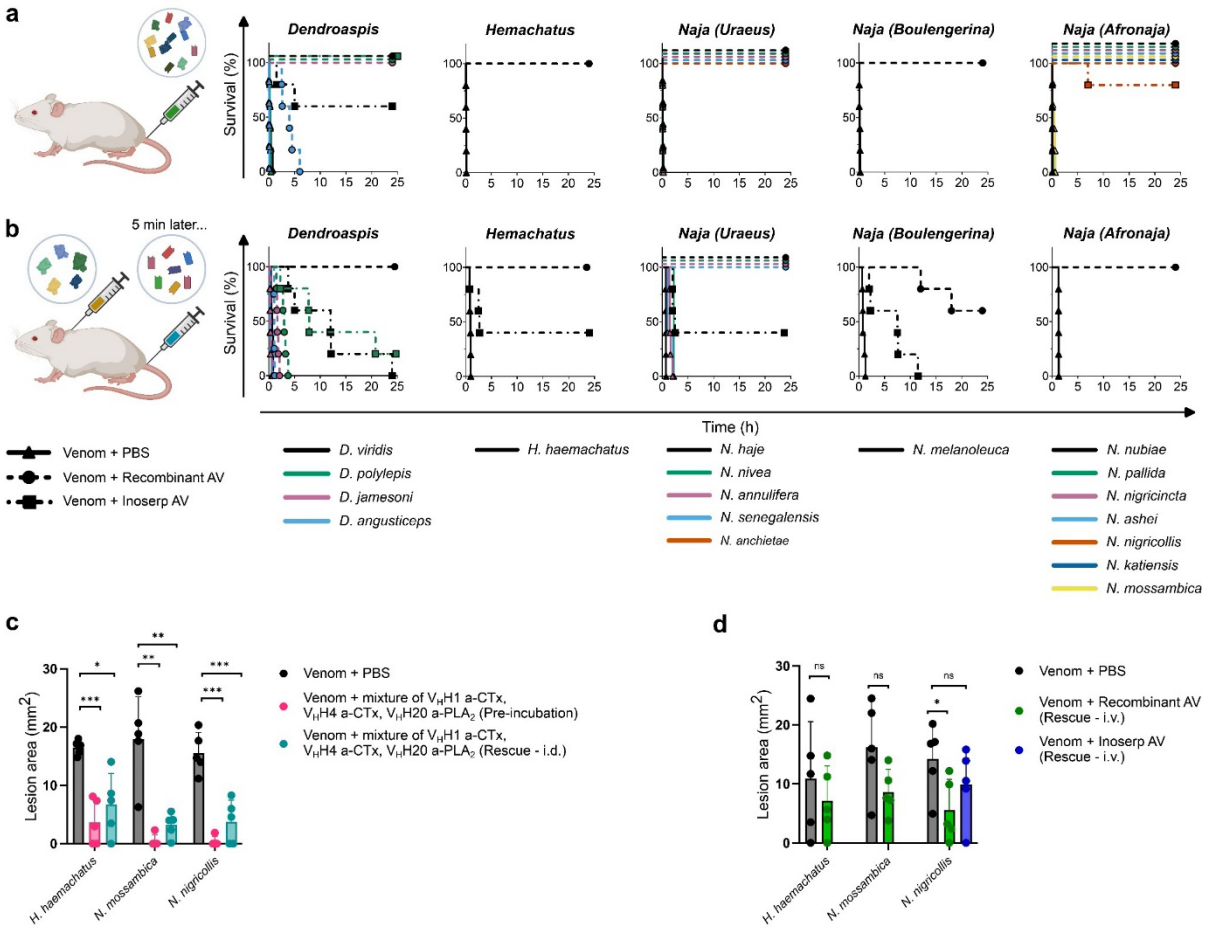

Fig. 5. *In vivo* neutralization of venom-induced lethality and dermonecrosis. **a,** Neutralization efficacy of the recombinant antivenom against venom-induced lethality caused by 18 elapid venoms in a pre-incubation setup. Venom and the recombinant antivenom were pre-incubated before i.v. injection. **b,** Neutralization efficacy of the recombinant antivenom against venom-induced lethality caused by 11 snake venoms in a rescue setup. Venom was injected s.c. followed by i.v. injection of the recombinant antivenom 5 minutes later. In both setups, Inoserp PAN-AFRICA antivenom was included for comparison. **c,** Neutralization of venom-induced dermonecrosis with a mixture of 3 V_HHs (V_HH1 a-CTx, V_HH4 a-CTx, and V_HH20 a-PLA_2) against 3 representative cytotoxic venoms from *H. haemachatus*, *N. mossambica*, and *N. nigricollis*, in both pre-incubation and rescue setups. In the pre-incubation setup, the V_HHs and venom were pre-incubated before i.d. injection, and in the rescue setup, the V_HH mixture was injected into the same region as the venom injection 15 minutes post-venom injection. The lesion size was measured 72 hours post-injection. **d,** The neutralization efficacy of the recombinant antivenom against dermonecrosis caused by the same 3 venoms in a second rescue setup. In this rescue setup, venom was injected i.d. and the recombinant antivenom was injected i.v. 15 minutes later. The lesion size was measured 48 hours post-injection. For *N. nigricollis* venom, in addition to the recombinant antivenom, Inoserp PAN-AFRICA antivenom was included for comparison.

Methods

Construction of an immune V_HH-displaying phage library

Immune V_HH-displaying phage libraries were constructed at the VIB nanobody core (Brussels, Belgium) as previously described.[20] To generate V_HH-displaying phage libraries, 1 alpaca and 1 llama were subcutaneously (s.c.) injected at bi-weekly intervals across 8 time points with increasing doses of venom mixtures from the 18 most medically relevant elapid snakes in sub-Saharan Africa, i.e. *Dendroaspis angusticeps*, *Dendroaspis jamesoni*, *Dendroaspis polylepis*, *Dendroaspis viridis*, *Naja anchietae*, *Naja annulifera*, *Naja ashei*, *Naja haje*, *Naja katiensis*, *Naja melanoleuca*, *Naja mossambica*, *Naja nigricincta*, *Naja nigricollis*, *Naja nivea*, *Naja nubiae*, *Naja pallida*, *Naja senegalensis*, and *Hemachatus haemachatus*. Following the initial series of injections, 3 additional booster injections were administered at 52, 54, and 60 weeks after the first immunization (Supplementary Table 2 summarizes the detailed immunization schedule). For library generation, blood samples were collected on days 5 and 8 following the first set of 4 injections. The 2 blood samples from each animal were pooled separately, and individual libraries were prepared for each animal. A total of 6 V_HH-displaying phage libraries, i.e. 1 library per time point and animal, were prepared by pooling the total RNA samples after days 46 and 49 (Library A), 102 and 105 (Library B), and days 5 and 8 following the final booster injections (Library C).

Purification and biotinylation of the venom fractions and toxins

Cardiotoxin (P01468) from *N. pallida*, α-cobratoxin (P01391) from *N. kaouthia*, α-short chain neurotoxin (P01426) from *N. pallida,* and whole venoms from the above-mentioned 18 elapid snakes were purchased in lyophilized form from Latoxan (Portes les Valence, France; Catalogue numbers and origin of the specimens can be found in Supplementary Table 1). Venom fractions containing short-chain neurotoxins (sNTx), long-chain neurotoxins (lNTx), cytotoxins (CTx), Og XI, AgTx, phospholipase A_2s (PLA_2), and dendrotoxins (DTx) were isolated from the whole venoms using reversed-phase high-performance liquid chromatography, RP-HPLC, (Agilent 1200) with a C_{18} column (250 × 4.6 mm, 5 µm particle; Teknokroma). 1 mg of venom solubilized in 100 µL Solution A (MilliQ water supplemented with 0.1% TFA) was applied to the column and elution was performed at a rate of 1 mL/min using Solution A and a gradient towards solution B (acetonitrile supplemented with 0.1% TFA): 0% B for 15 min, 0–15% B over 15 min, 15–45% B over 60 min, 45–70% B over 10 min, and 70% B over 9 min, as previously described.[73] Fractions were collected and the solvent evaporated using a vacuum centrifuge. The venom fractions purified via RP-HPLC and toxins bought from Latoxan were dissolved in phosphate buffered saline (PBS: 137 mM NaCl, 3 mM KCl, 8 mM $Na_2HPO_4{\cdot}2H_2O$, 1.4 mM KH_2PO_4, pH 7.4) and biotinylated by amine coupling using a 1:1 to 1:3 molar ratio of venom fraction or toxin to EZ-Link™ NHS-PEG_4-Biotin reagent (Thermo Scientific, A39259), as previously described.[35] Free biotin was removed using 2 or 4 kDa MWCO ultracentrifugation membranes (Vivacon® 500, VN01H91 and Amicon

Ultra-4, UFC8000324, respectively) in accordance with the manufacturers' guidelines. Following purification, the degree of biotinylation was analyzed by matrix-assisted laser desorption/ionization time-of-flight mass spectrometry (MALDI-TOF MS) using ProteoMass™ Protein MALDI-MS Calibration Kit (Sigma-Aldrich, MSCAL3) and an Ultraflex II TOF/TOF spectrometer (Bruker Daltonics), as previously described.[74]

Proteomics analysis of the selected venom fractions

From each venom fraction, 5 µg was diluted in 50 mM ammonium bicarbonate to a total volume of 25 µL. The samples were reduced and alkylated by 10 mM TCEP and 40 mM CAA before digestion with either GluC or trypsin in an enzyme-to-protein ratio of 1:100. Samples were incubated overnight at 37 ˚C, after which the digestion was stopped by addition of 2% TFA for a final concentration of 1%. The samples were desalted with SOLAµ SPE plate (HRP, Thermo) C18 columns, following the same procedure as previously described.[75] Dried peptides were reconstituted in 12 µL 2% ACN, 1%TFA, and an estimated 500 ng of peptides was used for MS analysis.

Peptides were loaded onto a 2 cm C18 trap column (ThermoFisher 164946), connected in-line to a 15 cm C18 reverse-phase analytical column (Thermo EasySpray ES904) using 100% solvent A (0.1% Formic acid in water) at 750 bar, using the Thermo EasyLC 1200 HPLC system, and the column oven operating at 35 °C. Peptides were eluted over a 35 min gradient ranging from 6 to 60% of solvent B (80% acetonitrile, 0.1% formic acid) at 250 nL/min, and the Q-Exactive instrument (Thermo Fisher Scientific) was run in a DD-MS2 top10 method. Full MS spectra were collected at a resolution of 70,000, with an AGC target of 3×10^6 or maximum injection time of 20 ms and a scan range of 300–1750 m/z. The MS2 spectra were obtained at a resolution of 17,500, with an AGC target value of 1×10^6 or maximum injection time of 60 ms, a normalized collision energy of 25 and an intensity threshold of 1.7×10^4. Dynamic exclusion was set to 60 s, and ions with a charge state <2 or unknown were excluded.

The raw data from all fractions were analyzed with Proteome Discoverer v2.4. The data were searched against all snake venom proteins (retrieved from Uniprot, 2,263 sequences, accessed 09/11/2021). The trypsin-digested fractions were searched with tryptic specificity, while the GluC-digested fractions were searched with GluC specificity, with 2 maximum missed cleavages allowed for both proteases. Minimum and maximum peptide lengths were set to 7 and 40, respectively. Precursor mass tolerance was 10 ppm, and fragment mass tolerance was 0.02 Da. Methionine oxidation (+15.995 Da) was set as dynamic modification, while initiator methionine loss (-131.040 Da), acetylation (+42.011 Da), or the combination of methionine loss and acetylation (-89.030 Da) were included as dynamic modifications for the protein terminus. Cysteine carbamidomethylation (+57.021 Da) was added as a static modification. Peptide-spectrum matching was performed with Sequest HT, and FDR control with Percolator (0.01 strict and 0.05 relaxed target FDR). FDR was also controlled at the peptide and protein levels with the same target FDRs. Proteins were quantified based on the unique and razor

peptides, using the Minora Feature Detector and the Precursor Ions Quantifier nodes with default settings, normalizing abundance to the total peptide amount in each MS run and scaling abundance values on the average of all runs.

Clustering toxins based on sequence identity

A sequence similarity network (SSN) was made with the Enzyme Function Initiative - Enzyme Similarity Tool (EFI-EST).[76,77] A fasta file containing the UniProt sequences of each discovered toxin from the whole venom of the included 18 elapid snakes was used by the tool to perform an all-by-all BLAST to obtain similarities between sequence pairs. Clustering of toxins with a minimum sequence identity of 70% was subsequently performed by using an alignment score threshold during SSN Finalization that corresponds to 70% identity in the "Percent Identity vs Alignment Score Box Plot" in the Dataset Analysis tab. The obtained SSN was visualized with Cytoscape.

Solution-based phage display selections

V_HH-displaying phage libraries were incubated with biotinylated venom fractions or toxins for 2 h at ambient temperature, with end over end rotation (Supplementary Table 3 summarizes the final concentration of target toxins and the libraries used in each selection round). Streptavidin coated Dynabeads (M-280, Fisher Scientific, 10465723) were blocked in PBS containing 3% non-fat dried milk powder for 1 h with end over end rotation, before addition to the target toxins mixed with the phage library. In each selection round, a background control was included where no antigen was mixed with the phage library. Subsequently, a KingFisher Flex system (Thermo Scientific, 711-82573) was used to wash the beads 3 times with PBST (PBS + 0.1% Tween) and 3 times with PBS, before eluting the bound phages in 120 µL of 0.1 mg/mL trypsin (Sigma-Aldrich, T9201-500MG) in phage elution buffer (50 mM Tris, 1 mM $CaCl_2$, pH 8.0). The eluted phages were amplified using the M13KO7 helper phage and concentrated by polyethylene glycol precipitation.

Subcloning, screening, and sequencing of V_HHs

Phagemids from the chosen selection outputs (Supplementary Table 3) were purified using the GeneJET™ Plasmid MiniPrep Kit (Thermo Fisher, K0503) according to the manufacturer's protocol. The V_HH-encoding genes were subcloned into the pBDS100 expression vector using the PstI and Eco91I restriction enzymes (New England Biolabs). Following transformation into the *E. coli* strain BL21 (DE3) (New England Biolabs), at least 184 individual colonies were picked from each chosen selection output and used for the expression of soluble V_HHs. Auto-induction media[78] was used to induce V_HH expression for 16 h at 30 °C. Thereafter, periplasmic cell extracts, containing soluble expressed V_HHs, were used for primary screenings in a previously described expression-normalized DELFIA (dissociation-enhanced lanthanide fluorescence immunoassay)[20] using 25 nM of target toxin. Clones with a signal intensity 10 times higher than the background (no addition of biotinylated target), were cherry-picked and went through a second round of screening in the expression-normalized DELFIA, against

multiple target toxins. For the cross-reactive clones, a dose-response experiment was performed, where the FLAG-tagged V_HHs in the periplasmic extracts were captured onto the anti-FLAG coated wells as described above; however, instead of a single concentration, a serial dilution of target toxins (1:1,000 nM) was added. Clones displaying a signal intensity 50 times over the negative control, and/or a low EC_{50} value in the dose response curves, were Sanger sequenced (Eurofins Genomics sequencing service) using the M13Rev primer (CAGGAAACAGCTATGAC). The V_HH frameworks and the complementarity determining regions (CDRs) were annotated using CLC Main Workbench (Qiagen) and the V_HHs with unique CDR sequences were produced for *in vitro* and *in vivo* assays.

Production of V_HHs for *in vitro* and *in vivo* experiments

For expression of V_HHs at scales up to 100 mL, the periplasmic extracts containing V_HHs were produced as described in the screening section, and then purified using Ni-resin (Sigma-Aldrich, P6611) via gravity flow. For larger-scale expressions (>250 mL), BL21 (DE3) cells, containing the plasmid encoding a unique V_HH, were cultivated as previously described.[20] Thereafter, the V_HH-containing supernatants were purified using immobilized metal ion affinity chromatography with a 2 mL column volume of Ni-NTA resin (HIS-select Nickel Affinity Gel, Sigma-Aldrich, P6611) equilibrated with PBS supplemented with 200 mM NaCl and 20 mM imidazole, pH 8.0. Elution was performed with PBS containing 200 mM NaCl and 135 mM imidazole, pH 8.0, followed by an overnight dialysis in SnakeSkin Dialysis Tubings (10 kDa MWCO, ThermoFisher Scientific, 68100) against PBS. Subsequently, V_HHs were concentrated using Amicon® Ultra-15 centrifugal filters (3 kDa MWCO, Fisher Scientific, 10781543).

Kinetic analysis of V_HHs using biolayer interferometry

The binding of V_HHs to the venom fractions and toxins was analyzed using biolayer interferometry (Octet-BLI; Octet RED 96, ForteBio). Biotinylated venom fractions and toxins at a concentration of 0.5 µg/mL were captured to a target spectral shift of 0.8 nanometer (nm) on a streptavidin coated BLI biosensor (Sartorius, 18-5020). A biosensor without antigen was included as a reference. V_HHs were prepared in running buffer (10 mM HEPES, 150 mM NaCl, 3 mM EDTA, 50 mM MES hydrate, and 0.05% P_{20} (MES-HEPES), pH 7.2). The toxin-loaded biosensors were dipped into 4 different V_HH concentrations (7.5, 30, 120, 480 nM) and a control without any V_HH. V_HH association was measured for 600 sec, followed by measuring V_HH dissociation in running buffer for 600 sec. Biosensors were regenerated by dipping into the regeneration buffer (10 mM Glycine, 4 M sodium chloride, pH 2.0) between each round, 5 times, for 10 sec each. For analysis, the reference BLI biosensor background was subtracted, a global model assuming a 1:1 interaction was used for fitting of the data, and calculations of kinetic parameters were all made in Octet Analysis Studio 12.2.2.26 (ForteBio).

Patch-clamp electrophysiology

Automated planar whole-cell patch-clamp experiments were performed as previously described.[20] All experiments were performed on a Qube 384 automated patch-clamp platform (Sophion Bioscience) with 384-channel, 10X mode patch chips (10 patch holes/site, site resistance 0.2 ± 0.04 MΩ). We used a human rhabdomyosarcoma cell line (American Type Culture Collection, ATCC) endogenously expressing muscle type nAChRs ($(\alpha_1)_2\beta_1\gamma\delta$) and 70 µM ACh for receptor activation. We first determined the IC_{80} value for the included toxins or venom fractions (sNTX-1, sNTx-3, sNTx-6, lNTx-3, lNTx-5, and lNTx-7) and used this concentration to evaluate the neutralization effect of the corresponding V_HHs. The V_HHs were used at molar ratios of 9:1 to 1:27 between toxin and V_HH. Finally, the inhibitory effect of the toxins on the elicited ACh current was normalized to the full ACh response and averaged in each group (n = 8). The data was analyzed with Sophion Analyzer v6.6.70 (Sophion Bioscience) and GraphPad Prism 10 software.

***In vitro* neutralization of cell cytotoxicity**

A cell viability assay was performed as previously described.[35] Briefly, N/TERT keratinocytes were seeded at 4,000 cells per well in 100 µL cell culture medium and incubated overnight under standard conditions. After determining the half-maximal inhibitory concentration (IC_{50}) of each venom, the cells were subjected to a venom concentration of 2 IC_{50}s, either in the absence or presence of a 1:5 molar ratio of CTx or PLA_2 to V_HH based on the CTx or PLA_2 contents of each venom[30], followed by a 24 h incubation step. Thereafter, the CellTiter-Glo luminescent cell viability assay (Promega, Madison, WI, USA) was performed in triplicate according to the manufacturer's protocol. A maximal cell death control was included, where the cell culture medium was supplemented with 0.01% Tween 20 to disrupt the cells. In addition, a maximum cell viability control was included, with cell culture medium supplemented with PBS, as well as a V_HH control, where cells were incubated with the highest tested V_HH concentration without venom, to confirm that the V_HHs alone do not affect cell viability. The data was visualized with GraphPad Prism 10 software.

***In vitro* neutralization of PLA_2 enzymatic activity**

Venom concentration inducing half of the maximum PLA_2 enzymatic activity (EC_{50}) was determined as previously described.[30] For inhibitory dose-response curves, V_HHs were diluted to 16 µM, followed by a 2-fold serial dilution in 10 steps. 50 µL of snake venom at a concentration of 4 EC_{50} values was mixed with the serial dilutions of the V_HHs and then incubated at room temperature for 30 min. The enzymatic reaction was started by adding 100 µL of 0.5 mM 4-nitro-3-(octanoyloxy)benzoic acid (NOBA) into the mixture. Final concentrations of the individual components in the enzymatic activity assays were 0.25 mM NOBA, and a 2-fold serial dilution of the V_HHs with the highest concentration set at 4 µM. After adding NOBA to the wells, plates were shaken at 300 rpm for 2 min, and then incubated at 37 °C for 40 min. Finally, the plates were centrifuged at 4,000 × *g* at 4 °C for 3 min, and absorbance was measured at 25 °C at 405 nm using a Multimode Microplate Reader (VICTOR

Nivo, HH35000500). The experiments were performed in duplicate and the absorbance averages were determined after subtracting a blank control containing no venom. The data was analyzed in Graphpad Prism 10 software with a nonlinear fit using 'Sigmoidal, 4PL, X is concentration'.

Co-crystallization of V_HHs and toxins

Lyophilized toxins and vacuum-dried venom fractions were reconstituted at 10 mg/mL in 5 mM Tris and 20 mM NaCl at pH 8.0. The toxins or venom fractions were then added to the V_HHs at a 3-fold molar excess (V_HH1 a-CTx : cardiotoxin (P01468), V_HH5 a-sNTx : α-short chain neurotoxin (P01426)) and incubated overnight at 4 °C. The V_HH:toxin complexes were purified using size-exclusion chromatography (Superdex 75 10/300GL column, Cytiva) on an NGC Quest™ 10 Plus Chromatography system (Bio-Rad) maintained at 4 °C, with the reconstitution buffer serving as the mobile phase. Before crystal screening, the V_HH:toxin complexes were concentrated to 15.0 mg/mL using 3.0 kDa MWCO ultracentrifugation filters (UFC500324, Merck).

Crystallization trials were performed at 21 °C via the sitting drop vapour diffusion method. Drops (0.3 µL) were set up at reservoir-to-protein ratios of 2:1, 1:1, or 1:2 in a 96-well drop format on SWISSCI MRC 2 well crystallization plates (JENA) using LMB, BCS, Index, and Structure screening solutions (Hampton Research). The wells were sealed with crystal clear tape and equilibrated against 50 µL of reservoir solution. The V_HH1 a-CTx co-crystal formed in 0.2 M ammonium acetate, 0.1 M sodium acetate, pH 4.6, 30% w/v PEG4000. The V_HH5 a-sNTx co-crystal formed in 0.2 M Sodium Chloride, 0.1 M sodium acetate, pH 4.6, 30% v/v MPD. The developed crystals were harvested using mounted CryoLoops (Hampton Research) with cryoprotection performed by adding glycerol to a neighbour drop with no crystals to a final concentration of 25%. The loop edge was kept in contact with the cryo solution for approximately 5 s to equilibrate before flash freezing the crystal in liquid nitrogen and shipping to the beamline for remote data collection. Final structural models and corresponding structure factors have been deposited in the Protein Data Bank (PDB) under accession codes: 9RIT and 9RIU.

Data collection and structure determination

X-ray diffraction data for the V_HH1 a-CTx and V_HH5 a-sNTx crystals were obtained at the Biomax (MAX IV synchrotron facility, Lund, Sweden) beamline. Complete datasets were collected over a 360° rotation for the V_HH1 a-CTx and V_HH5 a-sNTx crystals. The data processing was performed with XDSAPP3,[79-81] and the data is summarized in Supplementary Tables 10 and 11. Structures of the V_HHs in complex with their respective toxins were determined by molecular replacement with Phaser-MR[82] using an AlphaFold3 model for both the V_HH and the target toxin as a search model. Model building and refinement were performed with Phenix.refine[81] and Coot.[83]

The structures were evaluated using MolProbity with final statistics presented in Supplementary Tables 10 and 11. Molecular graphics were presented with PyMOL Molecular

Graphics System (Version 2.2r7pre, Schrödinger, LLC). Coordinates/structure factors have been submitted to the PDB database with the accession codes 9RIT and 9RIU.

Cryo-EM collection and processing

Cryo grids of V_HH20 a-PLA_2 in complex with PLA_2-3 were imaged at 190,000x nominal magnification using a Falcon 4i camera on a Glacios microscope at 200 kV. Automated image collection was performed using EPU from ThermoFisher. Images were aligned, dose-weighted, and Contrast Transfer Function (CTF)-corrected in the CryoSPARC LiveTM software platform, with automated image collection also performed using Smart EPU software (ThermoFisher). Data processing was carried out in CryoSPARC v4.5.3.[84] Blob particle picking was performed on all micrographs with a minimum particle diameter of 60 Å and a maximum of 90 Å. Particles extracted at 256 pixels box size were used to perform 2D classification, which were then used to generate a 3D reference model from ab initio refinement, followed by heterogeneous refinement and 3D classifications to obtain a good class that was further non-uniform (NU) heterogeneous refined. Gold-Standard Fourier Shell Correlation (GSFSC) resolution was calculated to be 5.4 Å. Due to the small size of the complex and the low resolution of the map, we could not build a model, but dock it in the AlphaFold3 predicted complex as an indicator of whether the predicted interface is plausible.

Generation of in silico predictions of V_HH:toxin complexes

For V_HH:toxin complexes that did not yield protein crystals, protein sequences were submitted as input to AlphaFold3 for structure prediction.[85] Multiple predictions were generated using randomized seeds for each V_HH:toxin complex. The model exhibiting the highest confidence scores (per-residue confidence estimate (pLDDT), predicted template modelling (pTM), and interface predicted template modelling (ipTM)) were selected for further analysis. Molecular visualization and graphic preparation were presented with PyMOL Molecular Graphics System (Version 2.2r7pre, Schrödinger, LLC).

***In vivo* neutralization of venom-induced lethality**

In vivo median lethal dose (LD_{50}) determinations and lethality neutralization experiments were conducted using groups of mice weighing 18 to 20 grams, comprising both sexes. At IBt-UNAM, the CD1 mouse strain was used in the experiments performed for designing the recombinant antivenom, LD_{50} value determinations, and rescue experiments. In experiments performed at the University of Northern Colorado (UNC), the NSA mouse strain was used for the pre-incubation assays. Time of death after administration of 3 LD_{50} values of venoms was recorded in both strains to secure homogeneous results. All mice were kept under 12 h light and dark cycles with food and water *ad libitum*. LD_{50} values were determined for selected toxins (lNTx-7 and sNTx-3) and all the target venoms using the intravenous (i.v.) route (Supplementary Table 6) as previously described.[20] In the case of venoms selected for rescue assays, LD_{50} values were also determined using the subcutaneous (s.c.) route (Supplementary Table 6).

Recombinant antivenom design experiments

To evaluate the neutralizing efficacy of the V_HHs and design a recombinant antivenom, neutralization of selected individual toxins and selected whole venoms was performed in pre-incubation experiments (Supplementary Fig. 4; Supplementary Table 7), as previously described.[20] The mice were observed during the first 3 h and then approximately every 6 h for signs of envenoming. The percentage of survival was determined 24 h after the injection and plotted as Kaplan-Meier survival curves using GraphPad Prism v10.2.

Pre-incubation experiments

For pre-incubation experiments of whole venoms, 3 LD_{50} values of each venom (Supplementary Table 6) were mixed with 3.6 mg (117 µL) of recombinant antivenom (Supplementary Table 8) in a total volume of 200 µL per mouse. This was then pre-incubated at 37 °C for 30 min before i.v. injection into groups of 5 mice. To compare the performance of the recombinant antivenom with a current plasma-derived commercial antivenom, 5 venoms were also tested for neutralization with the $F(ab')_2$ polyclonal antivenom Inoserp PAN-AFRICA (Lot # 5IT11003; expiration date November 2018) (INOSAN BioPharma, S.A.) which is currently recommended for the treatment of envenomings caused by 8 elapid and 5 viperid snakes from Africa. The antivenom was pre-incubated with the venom at 37 °C for 30 min, using the volume that neutralizes a minimum of 3 LD_{50} values of venom from *N. nigricollis* and *D. polylepis*, according to the manufacturer's product insert. This antivenom is also recommended for the treatment of bites by the elapid snakes *D. viridis, D. angusticeps, D. jamesoni, N. haje, N. pallida, N. melanoleuca, N. nivea* and *N. katiensis.* All mice were observed during the first 5 h and then approximately every 6 h for appearance of envenoming signs (Supplementary Table 9). The percentage of survival was determined 24 h after the injection and plotted as Kaplan-Meier survival curves using GraphPad Prism v10.2.

Rescue experiments

The venoms of 11 elapid snakes (*D. angusticeps, D. jamesoni, D. polylepis, D. viridis, N. annulifera, N. haje, N. melanoleuca, N. nivea, N. nubiae, N. senegalensis,* and *H. haemachatus*) were selected for their neutralization in rescue experiments. These were designed to better represent actual envenoming, where the venom is injected first (s.c.) and then the recombinant antivenom is administered using the i.v. route. In these experiments, 3 LD_{50} values of each of the selected venoms (Supplementary Table 6) were injected in a final volume of 40 µL PBS. The recombinant antivenom was injected 5 min later using the i.v. route in a total volume of 300 µL PBS. Since the recombinant antivenom was designed considering the LD_{50} value of each venom determined through i.v. administration, the dose of the recombinant antivenom used was adjusted based on the ratio between LD_{50} values determined through s.c. and i.v. injection for each venom. The mice were observed during the first 5 h and then approximately every 6 h for the appearance of envenoming signs. The percentage of survival was determined

24 h after the injection and plotted as Kaplan-Meier survival curves using GraphPad Prism v10.2

To compare the performance of the recombinant antivenom with a current plasma-derived commercial antivenom, rescue experiments were performed for some species (*D. jamesoni, D. viridis, N. haje, N. melanoleuca,* and *H. haemachatus*) using Inoserp PAN-AFRICA (Lot # 5IT11003; expiration date November 2018) (INOSAN BioPharma, S.A.). Similar to the pre-incubation experiments, the antivenom dose was the volume that, according to the manufacturer, neutralizes a minimum of 3 LD_{50} values of venom adjusted based on the ratio between the LD_{50} value determined by i.v. or s.c. injection.

Due to the low availability of commercial antivenom, a vial from an expired batch of Inoserp PAN-AFRICA was used for all experiments.

***In vivo* neutralization of venom-induced dermonecrosis**

For dermonecrosis experiments groups ($n \geq 5$) of male Swiss (CD1) mice (29-31 g) were used. Animals had ad libitum access to CRM irradiated food and filtered water. Prior to venom injection, mice were weighed and given 5 mg/kg subcutaneous morphine. The dorsal flanks of mice were shaved to monitor lesion progression.

Prevention of venom-induced dermonecrosis

For venom challenges, mice were injected intradermally (i.d.) in the ventral abdominal region, with venoms from *N. nigricollis* (24 µg/mouse), *N. mossambica* (39 µg/mouse), and *H. haemachatus* (26 µg/mouse) dissolved in 50 µL PBS. This dose corresponds to 1 Minimum Necrotizing Dose (MND), i.e. the dose which induces an area of dermonecrosis of 5 mm in diameter, 72 h after injection.[39] In pre-incubation models, 1 MND of venom from each of the 3 snakes was pre-incubated with 1.09 mg of a mixture of V_HH1 a-CTx (450 µg/mouse), V_HH4 a-CTx (450 µg/mouse), and V_HH20 a-PLA_2 (190 µg/mouse) at 37 °C for 30 min before i.d. injection. In the first rescue model, 1 MND dose of venom in 10 µL was injected i.d., followed by 1.09 mg of V_HHs in 40 µL at the same region after 15 min. In a second rescue model, 1 MND dose of venom was injected i.d. in a 50 µL volume, followed after 15 min by i.v. administration of 3.6 mg of recombinant antivenom (Supplementary Table 8) in 200 µL. For the control groups the same volume of PBS was administered instead of V_HHs. As a comparison, a group of mice received 1 MND of *N. nigricollis* venom followed by 4.2 mg of Inoserp PAN-AFRICA antivenom (INOSAN Biopharma).

Mice were monitored continuously for the first 6 h post-injection, with additional checks every 3 h up to 12 h and then 3 times daily up to 72 h in pre-incubation and i.d. rescue models and up to 48 h in i.v. rescue studies. At the end of each experiment, animals were humanely euthanized via inhalational CO_2. Lesions at injection sites were dissected, measured in 2 directions with digital calipers, and photographed with a camera and light ring.

Statistical Analysis

To evaluate the significance of outcomes from these experiments, a Welch t-test was used to compare mean lesion sizes between control and treatment groups, following confirmation that data met parametric assumptions. Normality was verified using the Shapiro-Wilk test, while 'ROUT' tests were performed to identify any outliers within the data. Comparisons were made against the negative control (PBS only). All analyses were conducted using GraphPad Prism (Version 10.3.1), with statistical significance set at $\alpha = 0.05$.

1 Chippaux, J.-P. Estimate of the burden of snakebites in sub-Saharan Africa: A meta-analytic approach. *Toxicon* **57**, 586-599, doi.org/10.1016/j.toxicon.2010.12.022 (2011).

20 Benard-Valle, M. *et al. In vivo* neutralization of coral snake venoms with an oligoclonal nanobody mixture in a murine challenge model. *Nature Communications* **15**, 4310, doi:10.1038/s41467-024-48539-z (2024).

30 Nguyen, G. T. T. *et al.* High-throughput proteomics and *in vitro* functional characterization of the 26 medically most important elapids and vipers from sub-Saharan Africa. *GigaScience* **11**, doi:10.1093/gigascience/giac121 (2022).

32 Kini, R. M. & Doley, R. Structure, function and evolution of three-finger toxins: Mini proteins with multiple targets. *Toxicon* **56**, 855-867, doi.org/10.1016/j.toxicon.2010.07.010 (2010).

35 Ahmadi, S. *et al.* An *in vitro* methodology for discovering broadly-neutralizing monoclonal antibodies. *Scientific Reports* **10**, 10765, doi:10.1038/s41598-020-67654-7 (2020).

38 Pucca, M. B. *et al.* Unity Makes Strength: Exploring Intraspecies and Interspecies Toxin Synergism between Phospholipases A_2 and Cytotoxins. *Frontiers in pharmacology* **11**, 611, doi:10.3389/fphar.2020.00611 (2020).

39 Petras, D. *et al.* Snake venomics of African spitting cobras: toxin composition and assessment of congeneric cross-reactivity of the pan-African EchiTAb-Plus-ICP antivenom by antivenomics and neutralization approaches. *Journal of proteome research* **10**, 1266-1280, doi:10.1021/pr101040f (2011).

65 Gutiérrez, J. M. *et al.* Snakebite envenoming. *Nature reviews. Disease primers* **3**, 17063, doi:10.1038/nrdp.2017.63 (2017).

66 Torres, S. V. *et al. De novo* designed proteins neutralize lethal snake venom toxins.

67 Segelke, B. W., Nguyen, D., Chee, R., Xuong, N. H. & Dennis, E. A. Structures of two novel crystal forms of *Naja naja naja* phospholipase A_2 lacking Ca^{2+} reveal trimeric packing Edited by I. A. Wilson. *Journal of Molecular Biology* **279**, 223-232, doi.org/10.1006/jmbi.1998.1759 (1998).

68 Hiu, J. J. & Yap, M. K. K. The myth of cobra venom cytotoxin: More than just direct cytolytic actions. *Toxicon: X* **14**, 100123, doi.org/10.1016/j.toxcx.2022.100123 (2022).

69 Gutiérrez, J. M. & Lomonte, B. Phospholipases A_2: Unveiling the secrets of a functionally versatile group of snake venom toxins. *Toxicon* **62**, 27-39, doi.org/10.1016/j.toxicon.2012.09.006 (2013).

70 Lou, X. *et al.* The Atomic Resolution Crystal Structure of Atratoxin Determined by Single Wavelength Anomalous Diffraction Phasing*. *Journal of Biological Chemistry* **279**, 39094-39104, doi.org/10.1074/jbc.M403863200 (2004).

71 Lancelin, J.-M., Foray, M.-F., Poncin, M., Hollecker, M. & Marion, D. Proteinase inhibitor homologues as potassium channel blockers. *Nature Structural Biology* **1**, 246-250, doi:10.1038/nsb0494-246 (1994).
72 Si, M., Trosclair, K., Hamilton, K. A. & Glasscock, E. Genetic ablation or pharmacological inhibition of Kv1.1 potassium channel subunits impairs atrial repolarization in mice. *American journal of physiology. Cell physiology* **316**, C154-c161, doi:10.1152/ajpcell.00335.2018 (2019).
73 Laustsen, A. H., Lomonte, B., Lohse, B., Fernández, J. & Gutiérrez, J. M. Unveiling the nature of black mamba (*Dendroaspis polylepis*) venom through venomics and antivenom immunoprofiling: Identification of key toxin targets for antivenom development. *Journal of proteomics* **119**, 126-142, doi:10.1016/j.jprot.2015.02.002 (2015).
74 Tulika, T. *et al.* Phage display assisted discovery of a pH-dependent anti-α-cobratoxin antibody from a natural variable domain library. *Protein science* **32**, e4821, doi:10.1002/pro.4821 (2023).
75 Rappsilber, J., Mann, M. & Ishihama, Y. Protocol for micro-purification, enrichment, pre-fractionation and storage of peptides for proteomics using StageTips. *Nature Protocols* **2**, 1896-1906, doi:10.1038/nprot.2007.261 (2007).
76 Oberg, N., Zallot, R. & Gerlt, J. A. EFI-EST, EFI-GNT, and EFI-CGFP: Enzyme Function Initiative (EFI) Web Resource for Genomic Enzymology Tools. *Journal of Molecular Biology* **435**, 168018, doi.org/10.1016/j.jmb.2023.168018 (2023).
77 Zallot, R., Oberg, N. & Gerlt, J. A. The EFI Web Resource for Genomic Enzymology Tools: Leveraging Protein, Genome, and Metagenome Databases to Discover Novel Enzymes and Metabolic Pathways. *Biochemistry* **58**, 4169-4182, doi:10.1021/acs.biochem.9b00735 (2019).
78 Studier, F. W. Protein production by auto-induction in high density shaking cultures. *Protein expression and purification* **41**, 207-234, doi:10.1016/j.pep.2005.01.016 (2005).
79 Krug, M., Weiss, M. S., Heinemann, U. & Mueller, U. XDSAPP: a graphical user interface for the convenient processing of diffraction data using XDS. *Journal of Applied Crystallography* **45**, 568-572, doi:10.1107/S0021889812011715 (2012).
80 Kabsch, W. XDS. *Acta crystallographica. Section D, Biological crystallography* **66**, 125-132, doi:10.1107/s0907444909047337 (2010).
81 Adams, P. D. *et al.* PHENIX: a comprehensive Python-based system for macromolecular structure solution. *Acta crystallographica. Section D, Biological crystallography* **66**, 213-221, doi:10.1107/s0907444909052925 (2010).
82 McCoy, A. J. *et al.* Phaser crystallographic software. *J Appl Crystallogr* **40**, 658-674, doi:10.1107/s0021889807021206 (2007).
83 Emsley, P., Lohkamp, B., Scott, W. G. & Cowtan, K. Features and development of Coot. *Acta crystallographica. Section D, Biological crystallography* **66**, 486-501, doi:10.1107/s0907444910007493 (2010).
84 Punjani, A., Rubinstein, J. L., Fleet, D. J. & Brubaker, M. A. cryoSPARC: algorithms for rapid unsupervised cryo-EM structure determination. *Nature Methods* **14**, 290-296, doi:10.1038/nmeth.4169 (2017).
85 Abramson, J. *et al.* Accurate structure prediction of biomolecular interactions with AlphaFold 3. *Nature* **630**, 493-500, doi:10.1038/s41586-024-07487-w (2024).